

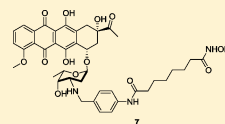
Dual Targeting of Histone Deacetylase and Topoisomerase II with Novel Bifunctional Inhibitors

William Guerrant,^{§,†} Vishal Patil,^{§,†} Joshua C. Canzoneri,^{§,†} and Adegboye K. Oyelere^{*,†,‡}

[†]School of Chemistry and Biochemistry, [‡]Parker H. Petit Institute for Bioengineering and Biosciences, Georgia Institute of Technology, Atlanta, Georgia 30332-0400, United States

S Supporting Information

ABSTRACT: Strategies to ameliorate the flaws of current chemotherapeutic agents, while maintaining potent anticancer activity, are of particular interest. Agents which can modulate multiple targets may have superior utility and fewer side effects than current single-target drugs. To explore the prospect in cancer therapy of a bivalent agent that combines two complementary chemo-active groups within a single molecular architecture, we have synthesized dual-acting histone deacetylase and topoisomerase II inhibitors. These dual-acting agents are derived from suberoylanilide hydroxamic acid (SAHA) and anthracycline daunorubicin, prototypical histone deacetylase (HDAC) and topoisomerase II (Topo II) inhibitors, respectively. We report herein that these agents present the signatures of inhibition of HDAC and Topo II in both cell-free and whole-cell assays. Moreover, these agents potently inhibit the proliferation of representative cancer cell lines.



Compound	HDAC 1 IC ₅₀ (nM)	HDAC 6 IC ₅₀ (nM)	HDAC 8 IC ₅₀ (nM)	DU-145 IC ₅₀ (μM)
7	47 ± 3	20 ± 1	220 ± 21	0.13
SAHA	38 ± 2	27 ± 2	1989 ± 156	2.12

INTRODUCTION

Several rational pharmacological strategies, including vaccination, gene therapy, immunotherapy, and new target identification and validation, have emerged for the treatment of metastatic diseases. Despite these progresses, chemotherapy remains the primary treatment of choice for most cancer cases. However, almost all chemotherapeutic agents suffer from severe toxicities and other undesirable side effects. To address these problems, the cancer medicine of the future will incorporate, within a single molecule, elements that allow for simultaneous targeting of multiple cancer-fighting targets while maintaining lower side effects.^{1–3} This realization has continued to spawn immense efforts in the literature. Studies aimed at identifying multivalent ligands as promising pharmacological tools that may be more efficacious for various human diseases than highly selective single-target drugs are ongoing in several academic and pharmaceutical laboratories.^{4–7} A subset of these studies has revealed that balanced modulation of a small number of targets may have superior efficacy and fewer side effects than single-target treatments.^{1,7,8}

Epigenetic control has become widely accepted as a mechanism for cell regulation.^{9–11} Specifically, histone deacetylase (HDAC) is a class of epigenetic enzymes that has generated much interest in cancer therapeutics literature. HDACs are known to associate with many oncogenes and tumor suppressors, leading to altered expression patterns, and have consequently become attractive targets for small-molecule inhibition.^{12,13} Histone deacetylase inhibitors (HDACi) have been shown to cause growth arrest, differentiation, and apoptosis in tumor cells and in animal models by inducing histone hyperacetylation and p21^{waf1} expression.^{14–17} Additionally, modulation of activities of HDACs alters the activity of a diverse range of proteins, many of which are attractive therapeutic targets

themselves, including p53, E2F, tubulin, and Hsp90.^{18–22} HDAC inhibition has been clinically validated as a therapeutic strategy for cancer treatment with the FDA approvals of suberoylanilide hydroxamic acid (SAHA) and romidepsin (FK-228) for treatment of cutaneous T cell lymphoma.^{23–25} However, a large number of the currently known HDACi have elicited only limited in vivo antitumor activities and have not progressed beyond preclinical characterizations.^{26–28} HDACi that modulate the functions of additional intracellular targets, other than the various HDAC isoforms, may be able to ameliorate many of the shortcomings of current inhibitors.

Because of the presence of large hydrophobic patches at the HDAC surface rim,^{29,30} it is conceivable that appropriate conjugation of the surface recognition group of a prototypical HDACi to other hydrophobic antitumor pharmacophores could furnish a new class of bifunctional agents. To date, there exist a few examples of this subtype of bifunctional HDACi derived compounds.^{31–33} Expansion of the repertoire of such bifunctional compounds could lead to broad acting, therapeutically viable anticancer agents.

An attractive starting point for a secondary target is the topoisomerase class of enzymes (Topo I and Topo II), which are validated targets for many small molecule inhibitors including clinically useful anthracyclines such as doxorubicin (DOX) and daunomycin or daunorubicin (DAU) (Figure 1) and camptothecins such as irinotecan and topotecan.³⁴ Topo inhibitors elicit anticancer activities primarily by stabilizing the DNA–enzyme cleavable complex through intercalation between DNA base pairs. However, DNA does not exist as a naked structure in the nucleus. It is noncovalently associated with

Received: March 25, 2011

Published: January 19, 2012

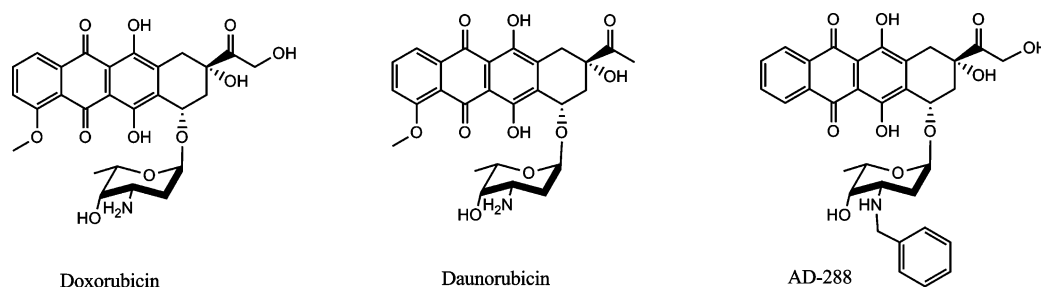


Figure 1. Representative structures of anthracycline antibiotics.

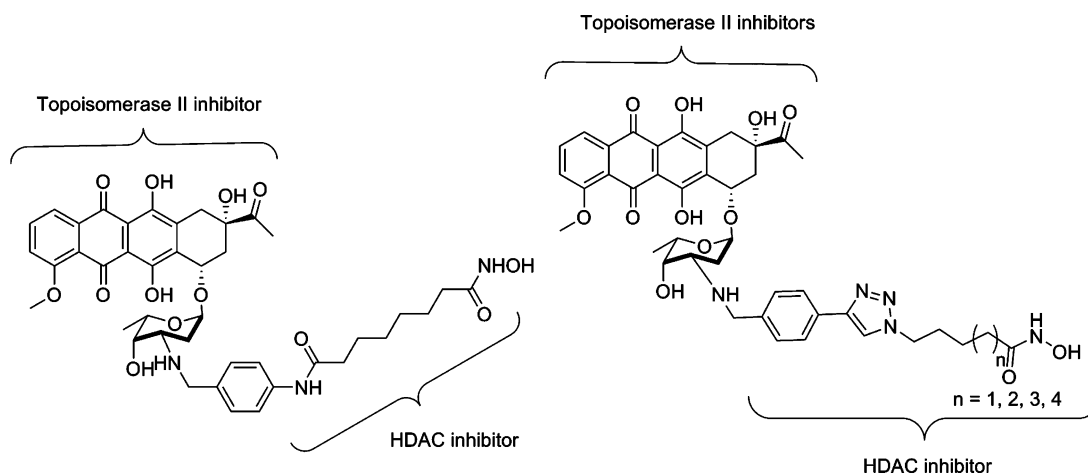


Figure 2. Design of dual-acting Topo II-HDAC inhibitors.

histones to form the nucleosomes which make up chromatin subunits. Agents, such as HDACi, that induce hyperacetylation of histone proteins complexed with DNA could increase the accessibility of DNA within chromatin and consequently potentiate the anticancer activities of Topo inhibitors.^{35,36} Moreover, recent observations have shown that HDAC1, HDAC2, and Topo II colocalize *in vivo* as part of functionally coupled complexes.^{37,38} These evidence suggest simultaneous Topo and HDAC inhibition could be a viable alternative approach in cancer therapy.

We disclose herein small molecules with dual acting Topo II-HDAC inhibitory activities. We found that many of these conjugates more potently inhibited HDAC and Topo II activities compared to SAHA and daunomycin, standard HDACi and Topo II inhibitors, respectively. Additionally, a subset of these compounds exhibited potent whole cell antiproliferative activities against representative breast, lung, and prostate cell lines.

RESULTS AND DISCUSSION

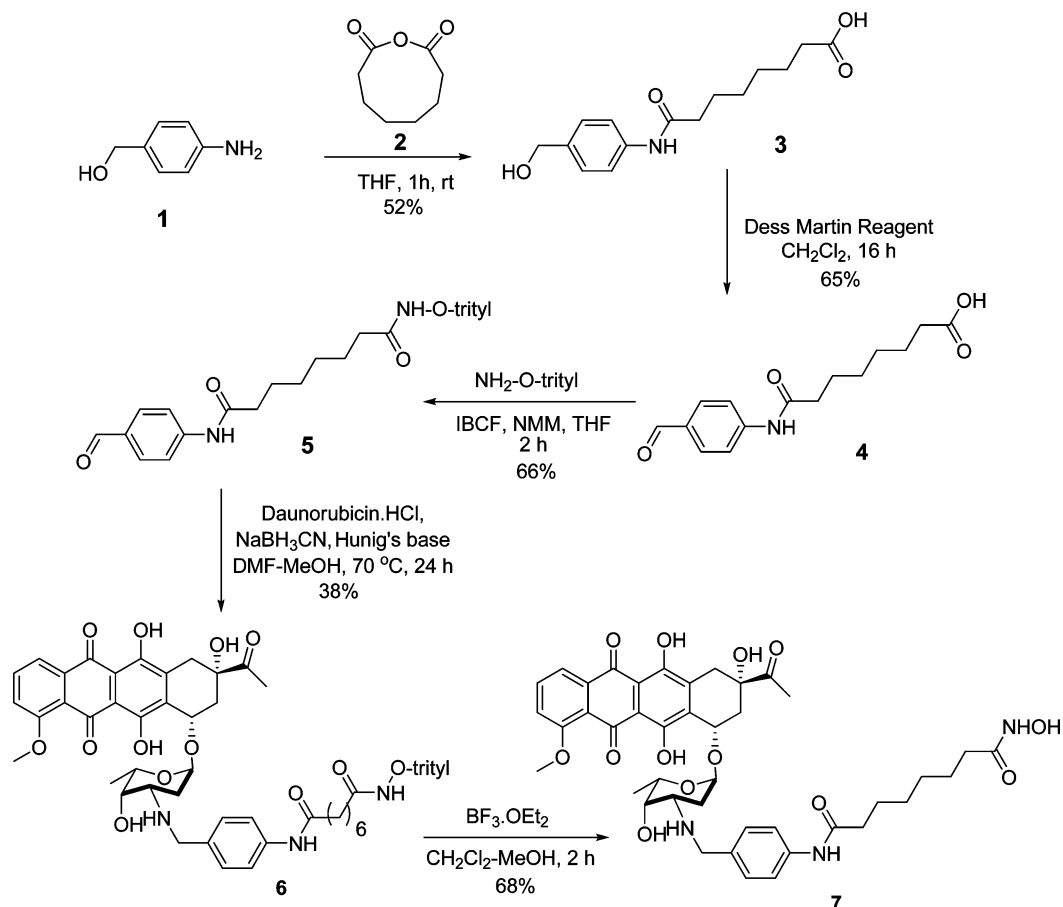
Design Rationale. Anthracyclines are one of the most thoroughly studied classes of anticancer agents with copious structure-activity relationship (SAR) data to aid the design and characterization of new anthracycline-containing compounds.³⁹⁻⁴⁴

Specifically, *N*-benzylated anthracyclines, such as *N*-benzyl doxorubicin (AD-288)⁴² (Figure 1), have enhanced Topo II inhibitory activities, reduced cardiotoxicity activity, and reduced susceptibility to the Pgp-mediated multidrug resistance.⁴⁵⁻⁴⁷ We postulated that introduction of the HDACi via *N*-benzylation of the DAU amino group would be compatible with Topo II inhibition and possibly engender the positive attributes of *N*-benzylated anthracyclines to the resulting conjugates. In turn,

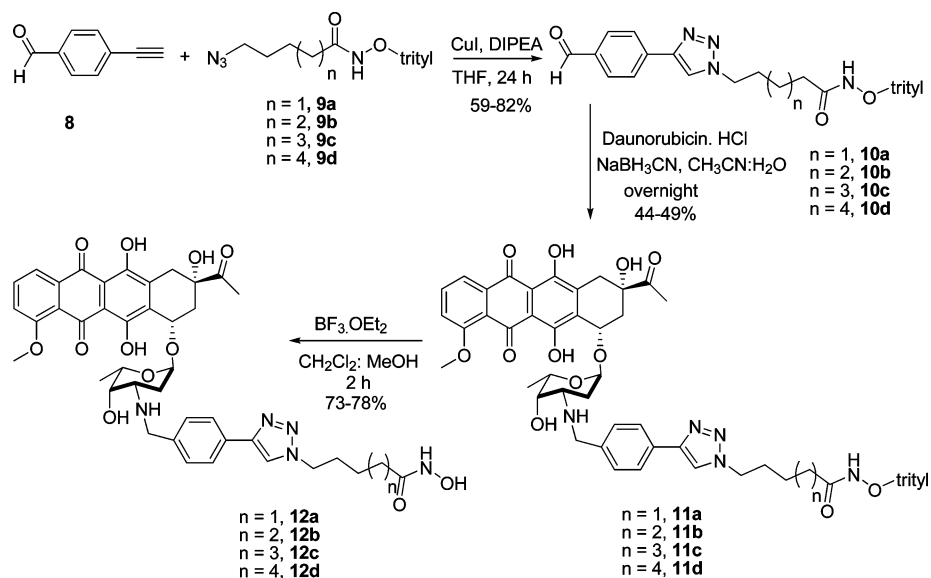
the anthracycline moiety could serve two other purposes: (i) as a surface recognition cap group, allowing favorable orientation of hydroxamic acid within the zinc binding pocket of HDAC, and (ii) as a delivery vehicle, because the transport of the anthracycline via proteasome could facilitate nuclear accumulation of HDACi.⁴³ On the basis of the forgoing, we designed two classes of conjugates: a direct DAU-SAHA conjugate and DAU-triazolylaryl hydroxamate conjugates (Figure 2). The later conjugates were inspired by our previous studies which revealed that triazole moiety could be incorporated in lieu of amide bond as a surface recognition connecting group in prototypical HDACi.⁴⁸

Chemistry. Crucial to the successful synthesis of all the conjugates described in this report is the reductive amination reaction between DAU and appropriate aldehyde intermediates **5** and **10a-d** (Schemes 1 and 2). Synthesis of aldehyde intermediate **5** started with the coupling of 4-aminobenzyl alcohol **1** to suberic anhydride **2** to give benzyl alcohol **3**. To assess the suitable oxidizing agent for conversion of alcohol **3** to aldehyde **4**, we employed MnO_2 , PCC, and Dess-Martin periodinane (DMP) oxidation. All yielded the desired aldehyde, with DMP giving the optimum yield among them. To synthesize the protected hydroxamate **5**, we coupled **4** to *O*-trityl hydroxylamine using standard EDC coupling chemistry. Interestingly, the amide bond of compound **4** was also susceptible to nucleophilic attack and led to a substantially lower yield under this condition. Using TBTU as coupling reagent resulted in the same outcome. Gratifyingly, the use of isobutylchloroformate (IBCF) as a coupling reagent gave coupled requisite product **5** in 66% yield within 2 h. Longer reaction times did not improve the yield and led to degradation of product. Reductive amination with DAU hydrochloride was the major hurdle in making the DAU-SAHA

Scheme 1. Synthesis of the SAHA-Based Dual-Acting Topo II–HDAC Inhibitor



Scheme 2. Synthesis of the SAHA-Like, Triazole-Based Topo II–HDACi



conjugate. Initial investigation with NaBH_3CN as a reducing agent with acetonitrile–water solvent system at room temperature led to a complex reaction mixture. Employing a non-aqueous solvent system, as well as a milder reducing agent such as $\text{NaBH}(\text{OAc})_3$, did not produce any detectable amount of product. Previous studies in the literature indicated that generation of free amine by addition of base and elevated temperature might

promote the imine formation.^{49,50} Indeed, adding Hunig's base to reductive amination reactions between DAU and aldehyde 5 in the presence of NaBH_3CN at 70 °C gave the desired coupled product 6, albeit in low yield. Reducing the reaction temperature to 50 °C and below worsened the yield, as did employing $\text{NaBH}(\text{OAc})_3$ as a reducing agent. The deprotection of the acid sensitive trityl group of compound 6 was accomplished by

treatment with the Lewis acid boron trifluoride etherate.⁵¹ This led to the removal of the trityl group to give the desired conjugate **7** in good yield without any need for further purification.

Similar chemistry was applied for the synthesis of triazole-based conjugates. The synthesis of requisite aldehydes **10a–d** started with Cu-catalyzed cycloaddition of 4-ethynylbenzaldehyde **8** with trityl-protected azido hydroxamates **9a–d** (Scheme 2). Reductive amination of triazole aldehydes **10a–d** with DAU proceeds readily at room temperature in aqueous solvent system to give the triazole-based conjugates **11a–d** in slightly improved yield compared to conjugate **6**. Boron trifluoride etherate deprotection of the trityl group of **11a–d** yielded the desired triazole-based conjugates **12a–d** in good to excellent yields.

In vitro HDAC Inhibition. We first tested the HDAC inhibition activity of compounds **7** and **12a–d** against crude HeLa cell nuclear extract HDACs using a cell free assay (Fluor de Lys) as previously described.⁴⁸ Overall, these compounds showed inhibition activities against HeLa cell nuclear extract HDACs, which are comparable to or exceed that of the standard SAHA (Table 1). It is particularly interesting that **7**

conjugates potently inhibit HeLa cell nuclear extract HDACs with IC_{50} in the low to midnanomolar range. Among these conjugates, **12a** is the least active, closely followed by **12d**, which is about 20-fold more potent. Compounds **12b** and **12c** have the most potent anti-HDAC activity, with a slight preference for the six methylene-linked **12c**. Interestingly, the triazole-linked compound **12b** is 40-fold more potent than the amide-linked **7** despite their similar linker length. Relative to the standard SAHA, **12c**, the most potent compound in this series, is 70-fold more potent (Table 1). The foregoing results showed that these conjugates followed a trend similar to that which we noted for the previously reported, structurally unrelated, triazole-based HDACi.⁴⁸

To obtain evidence for the HDAC isoform selectivity, we tested these dual acting Topo II–HDACi conjugates against selected recombinant HDACs—HDAC 1, HDAC 6 and HDAC 8. The pattern of the anti-HDAC activities of these compounds against HDAC 1 and HDAC 6 is similar to what we observed for the HeLa cell nuclear extract HDACs with few exceptions. Specifically, compounds **7** and **12b** have indistinguishable activity against HDAC 1 and HDAC 6 (Table 1). Additionally, **12a** which has midnanomolar IC_{50} against HeLa cell nuclear extract HDACs is almost inactive against HDAC 1 ($IC_{50} = 4.6 \mu M$) while it maintains decent activity against HDAC 6 ($IC_{50} = 0.6 \mu M$). We are not exactly sure of the cause of this disparity. In general, these compounds are weaker inhibitors of HDAC 8 with the exception of **7**, whose anti-HDAC 8 activity is only about 4-fold less than its anti-HDAC 1 activity (Table 1). These data suggest that **7** is a more indiscriminate inhibitor of these sets of HDACs while the rest of the conjugates are more selective.

Molecular Docking. To obtain information on the structural basis of the observed disparity in the HDAC inhibitory activity of these compounds, we performed molecular docking using a validated molecular dock program (AutoDock)^{48,52} Docking analysis was performed on a HDAC 1 homology model built from human HDAC 2 X-ray structure 3MAX coordinates.⁵³ We chose to dock the compound which had the least HDAC inhibitory activity (**12a**) and the compound which had the best HDAC inhibitory activity (**12c**) to delineate the basis of the ~600 fold activity difference between the two.

Table 1. In Vitro HDAC Inhibition

compd	<i>n</i>	HDAC 1/2 IC_{50} (nM) ^a	HDAC 1 IC_{50} (nM) ^b	HDAC 6 IC_{50} (nM) ^b	HDAC 8 IC_{50} (nM) ^b
SAHA		65.0	38 ± 2	27 ± 2	1989 ± 156
DAU		ND	NT	NT	NT
7		64.7	47 ± 3	20 ± 1	220 ± 21
12a	1	89.9	4600 ± 240	555 ± 36	ND
12b	2	1.6	54 ± 3	30 ± 2	4,129 ± 421
12c	3	0.9	8 ± 0.4	20 ± 0.4	710 ± 43
12d	4	4.2	11 ± 0.4	19 ± 1	379 ± 37

^aInhibition was assayed using the Biomol HDAC Fluorimetric Assay/Drug Discovery Kit. ^bData obtained through contract arrangement with BPS Bioscience (San Diego, USA; www.bpsbioscience.com).

has identical anti-HDAC activity to SAHA. This result suggests that the attachment of DAU does not impair the interaction between the HDACi component of the conjugate and the HDAC enzyme outer surface residues. It is also conceivable that the conjugate may adopt a conformation whereby the anthracycline moiety can contribute positively to the interaction with the crucial active site or surface residues. All triazole-linked

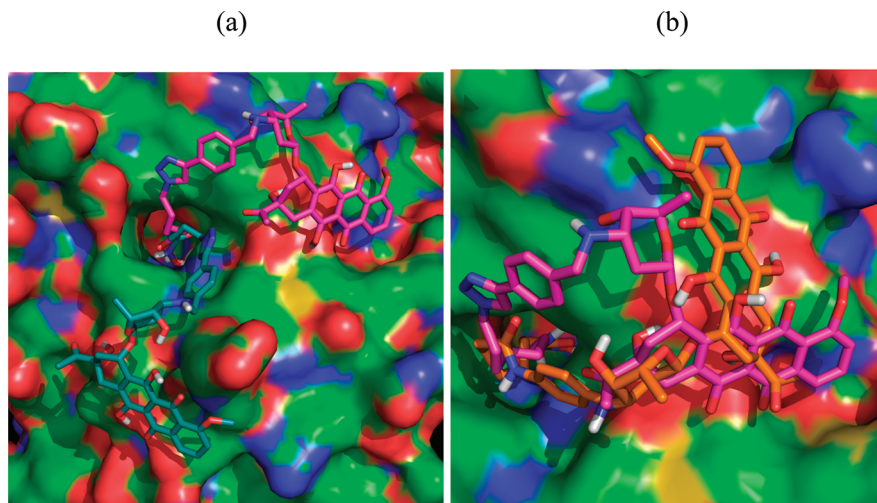


Figure 3. Docked structure of Topo II–HDACi conjugates at HDAC 1 active site. (a) Superposition of low energy conformations of **12a** (teal) and **12c** (pink). (b) Overlay of low energy conformations of **12c** (pink) and **7** (orange).

Additionally, we performed docking on compound **7** because of its distinct structural feature compared to **12a–12c**.

Interestingly, compound **12a** and **12c**, differing only in linker length, do not bind to the same pocket but instead localize to two different pockets (Figure 3a). For six-methylene-linked compound **12c**, the hydroxyl group of the daunosamine sugar could potentially make hydrogen bonding contact with the guanidinium group of Arg270 and the linker region could facilitate the presentation of the hydroxamic acid to the catalytic zinc by entering through the top of the hydrophobic channel that leads to the active site (Figure 3a and Supporting Information Figure S1c, d). In addition, two of the hydroxyl groups from the anthracycline ring of **12c** could take part in the H-bonding interaction with the backbone carbonyl group of Arg270 and the N–H group of Gly272. Possibly to accommodate the shorter linker length, **12a** loses the H-bonding interaction between the hydroxyl group of its daunosamine sugar and the enzyme's Arg270. Although other hydroxyl groups of the **12a** anthracycline ring make potentially compensatory H-bonding contacts with the phenolic group of Tyr201 and the backbone carbonyl groups of Gly207 and Pro206 (See Supporting Information Figure S1a, b), its binding pocket is more solvent-exposed, compared to the binding pocket of **12c** (Figure 3a).

Compound **7** binds close to the same pocket as **12c**; it however derives its binding affinity through different sets of interactions. Unlike **12c** which enters the active site associating with the top of the hydrophobic channel, **7** traverses the same channel more closely associated with residues on the opposite side of the channel (Figure 3b). Consequently, the daunosamine hydroxyl group of **7** could not interact with Arg270 in a similar way as that of **12c**. In lieu of this interaction, the anthracycline ring of **7** may engage in other H-bonding interactions with the backbone carbonyl groups of Gly272, Gly268, and Thr304 on the enzyme surface rim (Figure 3b and Supporting Information Figure S1e, f). These apparent differences in the binding orientation at the enzyme surface rim could account for the disparity in the potency of compounds **7**, **12a**, and **12c** against HDAC 1.

In Vitro Topoisomerase II Decatenation. We performed a cell-free DNA decatenation assay to determine the Topo II inhibition activity of these Topo II–HDACi conjugates. We used kinetoplast DNA (KDNA), a catenated network of mitochondrial DNA seen in trypanosomes, to quantify the conjugates' Topo II inhibition activity according to a literature protocol.^{54,55} Figure 4 illustrates the results obtained from this

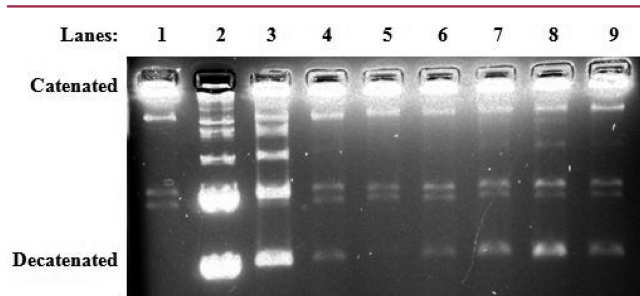


Figure 4. Topoisomerase II decatenation assay. Lanes 1–3: (1) KDNA, (2) decatenated KDNA marker, (3) KDNA and Topo II. Lanes 4–9: KDNA, Topo II, and 50 μM (4) DAU, (5) **12c**, (6) **12b**, (7) **12d**, (8) **12a**, (9) **7**.

study. KDNA and decatenated KDNA marker (lanes 1 and 2, respectively) were used as controls. Treatment of KDNA with

Topo II within 10 min at 37 $^{\circ}\text{C}$ resulted in an extensive DNA decatenation (lane 3). As expected, addition of 50 μM DAU to the decatenation experiment resulted in a severe impairment of DNA decatenation (comparing lanes 3 and 4). Relative to DAU, **12a** and **12d** have lower Topo II inhibition activity, with the worst overall inhibition shown by **12a**, the conjugate with a four-methylene linker (lanes 7 and 8). Conjugates **12b** and **7** inhibited Topo II activity at comparable levels to that of DAU at the same drug concentration (lanes 6 and 9, respectively). However, compound **12c** had an enhanced Topo II inhibition activity relative to DAU, resulting in a near total inhibition at 50 μM (comparing lanes 4 and 5). These results show that the Topo II inhibition activity of DAU is tolerant of an appropriate attachment of HDACi groups and, as in the case of **12c**, such groups could further enhance Topo II inhibition activities of anthracycline derivatives. The molecular basis of the HDACi linker length-dependent enhancement of Topo II inhibition of these dual-acting conjugates is not entirely clear. It is plausible that the placement of the HDACi group of these conjugates within DNA minor grooves, through the daunosamine sugar,⁵⁶ could further promote drug–DNA association, thereby enhancing the stability of the biologically relevant drug–DNA–Topo II ternary complex. Interestingly, **12c** also has the most potent inhibition activity against HDAC 1 (Table 1). It is exciting to observe that a single compound could embody optimum anti-HDAC and Topo II inhibition activities under these cell-free conditions.

In Vitro Cell Growth Inhibition. Cell viability experiments were performed to probe for the prospect of biological activity of these compounds in the cellular milieu. Three human cancer cell lines were used to quantify IC_{50} values for these compounds. Table 2 shows the IC_{50} values of each compound for

Table 2. Cell Viability Assay

compd	<i>n</i>	DU-145 IC_{50} (μM) ^a	SK-MES-1 IC_{50} (μM) ^a	MCF-7 IC_{50} (μM) ^a
7		0.13 \pm 0.06	0.47 \pm 0.02	0.99 \pm 0.21
12a	1	5.39 \pm 1.02	15.3 \pm 3.1	24.5 \pm 1.6
12b	2	1.61 \pm 0.29	4.68 \pm 0.75	13.4 \pm 1.85
12c	3	2.92 \pm 0.31	3.31 \pm 0.23	10.6 \pm 0.94
12d	4	2.06 \pm 0.33	2.61 \pm 0.11	14.8 \pm 1.6
DAU		0.09 \pm 0.002	0.17 \pm 0.09	0.95 \pm 0.05
SAHA		2.12 \pm 0.25	2.42 \pm 0.38	2.50 \pm 0.61

^aValues are the average of two experiments performed in triplicate. IC_{50} values were determined using the MTS assay (Promega).

all cancer cell types studied. The positive control compounds DAU and SAHA inhibit the proliferation of these tumor cell lines with IC_{50} similar to the values in the literature.^{57,58} DAU displays cell line dependent cytotoxicity that varies by as much as 10-fold among these three cell lines while SAHA shows no such cell line dependent effect (Table 2). Bifunctional compounds **12a–d** show linker length dependent antiproliferative activities that closely matched their anti-HDAC activities. Among the three transformed cell lines investigated, these compounds decreased the viability of DU-145 the most, while they are least cytotoxicity against MCF-7. Although less pronounced than that seen with DAU, these compounds display cell line-dependent cytotoxicity as well. Nevertheless, the micromolar IC_{50} values and the traction with anti-HDAC activities suggest that HDAC inhibition is the dominating mode of antiproliferative activities of compounds **12a–d**. Specifically, the

antiproliferative activities of **12c** and SAHA, compounds with similar linker length, are virtually indistinguishable against DU-145 and SK-MES-1 cell lines. This finding is surprising because **12c** displays the most potent HDAC and Topo II inhibition activities. Interestingly, compound **7**, a true hybrid between SAHA and DAU, showed the best cytotoxicity of all the bifunctional compounds across all cell lines, possessing sub-micromolar activities. In fact, the cytotoxicity of **7** closely rivals that of DAU, and they are equipotent against MCF-7. This is contrary to the trend seen in the cell-free assays. The potentiation of the activity of **7** within the cellular environment could be due to many factors, including the predominance of the Topo II inhibition character in dictating the bioactivity of **7**, the indiscriminate inhibition of multiple HDAC isoforms, or an alternative mechanism(s) that is unrelated to the inhibition of the activities of either target.

Histone Hyperacetylation and p21^{waf1} Expression. To gain a better perspective of the molecular mechanism of the antiproliferative activities of these dual-acting inhibitors, we probed the effect of their exposure on the intracellular status of p21^{waf1} (p21) protein in DU-145 prostate cancer cells. p21 has been shown to be upregulated in response to HDACi treatment, as well as in a p53-independent response to DOX.^{59,60} We dosed inhibitors at concentrations near the determined IC₅₀ in DU-145 and evaluated protein expression status using Western blotting (Figure 5). We controlled for equivalent protein loading using

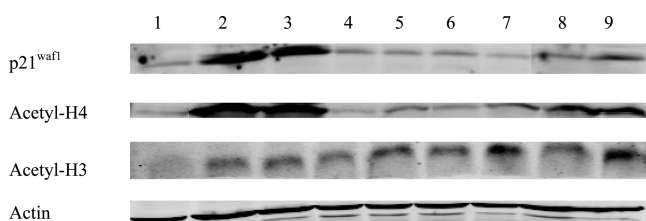


Figure 5. Immunoblot detection of cellular HDACi Markers. DU-145 cells were dosed for 24 h at the indicated concentrations to probe for acetylated histones H4 and H3, and p21^{waf1}. Actin was also probed to show equal loading of protein. Lane: (1) control; SAHA (2) 2.5 μM, (3) 5 μM; DAU (4) 0.1 μM, (5) 0.5 μM; **7** (6) 0.5 μM, (7) 1 μM; **12b** (8) 2.5 μM, (9) 5 μM.

antiactin antibody (Figure 5, bottom panel). As expected, SAHA results in marked upregulation of p21, even at 2.5 μM (top panel, lanes 2 and 3). However, neither DAU nor **7** shows noticeable upregulation in p21 expression compared to control levels (top panel, comparing lanes 4–7 to lane 1). This trend is reversed with **12b**, as a dose-dependent upregulation of p21 expression was observed (top panel, lanes 8 and 9). Relative to SAHA, however, the extent of p21 upregulation by **12b** is lower, although both were dosed at the same concentrations. Because these experiments were done at the IC₅₀ of the respective compounds, these results may indicate that **7** and **12b** derived their cytotoxic activity primarily through Topo II and HDAC inhibition, respectively. Alternatively, the cytotoxic activity **7** could be due to perturbation of other intracellular HDAC inhibition markers.

To further investigate into the prospect of distinct mechanisms of action for **7** and **12b**, we probed for histone acetylation status in DU-145 cells exposed to the same drug concentrations used for p21 immunoblotting. Intracellular histone acetylation status is a more direct indicator of class I HDAC inhibition. SAHA shows a strong histone H4 acetylation

(Figure 5, second panel, lanes 2 and 3), while DAU and **7** display moderate dose-dependent change in acetylation at the concentrations tested (2nd panel, lanes 4–7). Compound **12b** shows a strong H4 acetylation, with levels close to that of SAHA, at both concentrations (2nd panel, lanes 8 and 9). The trend of the drug induced perturbation of the acetylation state of H3, in core histones purified by acid extraction of DU-145 cell nuclear extract, is similar to what obtained for H4. Relative to the control, we observed distinct H3 hyperacetylation in DU-145 cells exposed to the same drug concentrations used for H4 immunoblotting (Figure 5, third panel). These results provide evidence supporting the involvement of intracellular HDAC inhibition as part of the mechanisms of bioactivity of the dual acting compounds **7** and **12b**.

Tubulin Acetylation. Additional data was sought in order to clarify the mechanisms involved in the antiproliferative activities and to delineate the disparity in enzyme inhibition versus antiproliferative activity. Tubulin was chosen as a target because it is acetylated by the cytoplasmic HDAC6,^{21,61,62} for which **7** and **12b** had nearly identical inhibition. Interestingly, inhibition of HDAC6-associated tubulin acetylation has been shown to enhance the cytotoxicity of DNA-damaging agents.⁶³ While most HDACi induce p21^{waf1} overexpression, inhibition of tubulin deacetylation is compound specific,⁶⁴ potentially allowing for differentiation between the mechanisms and potencies of **7** and **12b**. Because tubulin acetylation in response to HDACi is a relatively early event,⁶⁵ we dosed DU-145 cells for 4 h with inhibitors at either IC₅₀ concentrations (Table 2) or a high concentration (~5× IC₅₀). Immunoblotting revealed highly varied levels of tubulin acetylation among the inhibitors. DAU induced the lowest levels of acetylation, with IC₅₀ concentration showing levels comparable with control and only a slight increase in response to higher concentration of drug (Figure 6,

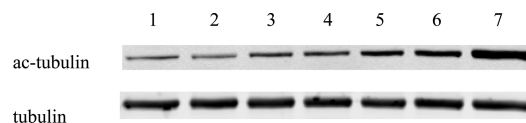


Figure 6. Tubulin acetylation in response to TopoII-HDACi. DU-145 cells were dosed for 4 h with: (1) control (0.1% DMSO), (2) DAU 90 nM, (3) DAU 500 nM, (4) **7** 130 nM, (5) **7** 500 nM, (6) **12b** 1.31 μM, (7) **12b** 10 μM.

lanes 1–3). Compound **7** induced moderate levels of acetylation (Figure 6, lanes 4 and 5), while **12b** caused robust acetylation at 5× its IC₅₀ (Figure 6, lanes 6 and 7). p21 expression at 4 h remained low across all compounds tested, with no discernible induction relative to control (data not shown).

Intracellular Topoisomerase II Inhibition. To obtain information about the intracellular fate of Topo II upon cell exposure to these dual-acting agents, we used an immunoblotting kit to assay compound-induced Topo II inhibition in an intracellular environment (Figure 7).⁶⁶ DU-145 cells were dosed with drug concentrations corresponding to cell growth inhibition IC₅₀s, while the control cells were dosed with vehicle (0.1% DMSO). The relative levels of stabilized Topo II–DNA cleavage complexes were determined for a 30 min drug treatment, as described by the manufacturer. Within this period, the control cells showed no significant amounts of Topo II inhibition, evidenced by the low levels of Topo II associated DNA (Figure 7a, lane 1). Cells treated with DAU and **12b** contained high levels of Topo II–DNA cleavage complexes,

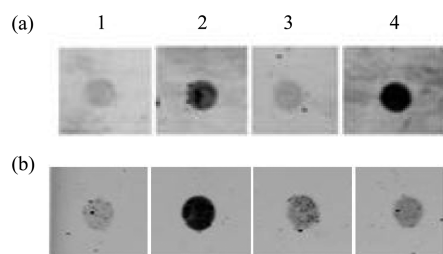


Figure 7. Intracellular Topo II Inhibition. DU-145 cells were probed for stabilized DNA–Topo II cleavage complexes upon (a) 30 min treatment; (b) 72 h treatment with bifunctional compounds: (1) control, (2) 90 nM DAU, (3) 130 nM 7, (4) 1.6 μ M 12b.

with **12b** showing a significantly higher amount (Figure 7a, lanes 2 and 4, respectively). This result suggests that **12b** could derive its cytotoxic activity, in part, from intracellular Topo II inhibition. Conversely, the levels of Topo II–DNA cleavage complexes in cells exposed to **7** is indistinguishable from that of the control cells (Figure 7, lane 3), suggesting a minimal contribution of Topo II inhibition to the cytotoxic activity of **7** within this period. This observation is surprising in light of the seemingly contradictory moderate effect of **7** on H4 hyperacetylation (Figure 5), tubulin acetylation (Figure 6), and its potent cell growth inhibition activity (Table 2).

To elucidate any contribution Topo II inhibition could be adding to long-term inhibition of cell proliferation, Topo II cleavage complexes were assayed after 72 h of treatment with compounds (Figure 7b). As expected, DAU treatment results in significant inhibition of Topo II activity relative to control levels (Figure 7b, comparing lanes 1 and 2). Compound **7** shows a measured increase in Topo II inhibition relative to control levels (Figure 7b, comparing lanes 1 and 3). Interestingly, we observed a drastic drop in the levels of stabilized Topo II–DNA cleavage complexes upon cell exposure to **12b** for 72 h (comparing lane 4 of parts a and b of Figure 7). This result suggests that the Topo II inhibition activity of **7** increases with time while that of **12** decreases. The persistence of the stabilized Topo II–DNA cleavage complexes over a longer period indicates that Topo II inhibition may contribute significantly to the mechanism of the antiproliferative activity of **7**.

Cellular Localization. HDAC1 and Topo II are cell nucleus-localized targets of these bifunctional compounds, while HDAC6 is cytoplasmic. To probe if cell penetration issues could be one of the alternative reasons for the difference in the potencies of compounds **7** and **12b**, we used confocal microscopy to visualize their intracellular localization (Figure 8). We exposed DU-145 cells to 1 μ M of DAU, **7** and **12b**. After 4 h incubation time, cells were monitored at 488 nm, the excitation wavelength (λ_{ex}) of

DAU, and we observed clear differences in the intracellular distribution profiles of the tested compounds. In agreement with previous study in the literature,⁶⁷ DAU is localized within the nuclear and perinuclear regions of DU-145 cells. Although it shows a less nuclear localization, compound **7** is more widely distributed within the cytosol, with evidence for perinuclear localization in similar manner to that of DAU. In contrast, **12b** shows a highly diminished intracellular distribution, with the bulk of the compound trapped in vesicle-like bodies within the cell (Figure 8). The relatively poor intracellular distribution of **12b** could be due to low cell membrane penetration or an enhanced pump-induced efflux of compound from within the cell.⁶⁸ We obtained a similar result with a lung tumor derived A549 cells (Supporting Information Figure S2). These results show that **7** and **12b** have different intracellular residency, which may affect access to their targets and consequently offer additional insight into underlying factors that could contribute to the disparity in the *in vitro* potency of these compounds.

CONCLUSION

There is evidence for the synergistic effect of combined Topo II and HDAC inhibitors on cancer.³⁸ However, this synergy is schedule dependent, hence traditional combination therapy involving Topo and HDAC inhibitors may be complicated by the inherent pharmacokinetic disadvantage of two separate drugs. To critically delineate the benefits of simultaneous Topo and HDAC inhibition in cancer therapy, it will be of interest to identify agents that possess Topo and HDAC inhibition activities within a single molecule. Toward this end, we have created dual-acting Topo II–HDAC inhibitors. A subset of these compounds potently inhibits the proliferation of representative cancer cell lines. When subjected to target-specific screening, these agents present both HDAC and Topo II inhibition signatures under cell-free conditions and in *in vitro* cell cultures. This observation suggests that the cytotoxic activities and potency of these dual-acting compounds could be dictated by either of the two antitumor pharmacophores. Specifically, results from HDAC and Topo inhibition studies, and p21, acetyl-H4, and acetyl-tubulin immunoblots highlight compound **7** as a moderate, yet sustained modulator of several intracellular targets important in tumor etiology. This may explain the superior antitumor activity of compound **7** relative to the other dual acting agents disclosed in this study. It is, however, instructive to emphasize that the target validation experiments described herein are performed under different conditions at different incubation periods, so parsing out the specific contributions of the two targets to the bioactivity of these agents may not be direct.

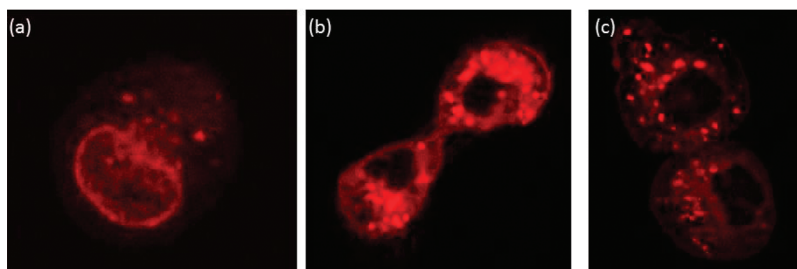


Figure 8. Cellular localization of dual-acting inhibitors. (a) DAU, (b) **7**, (c) **12b**. DU-145 cells were dosed at 1 μ M for 4 h with indicated compounds and visualized by confocal microscopy.

Another target-independent factor which influences the bioactivity of the anthracycline-derived dual-acting agent is their cell uptake and/or residency. In fact, diminished intracellular residency, occasioned by multidrug resistance protein (MRP) mediated efflux, is one of the problems of an anthracycline based chemotherapy regimen.⁶⁸ Compound **12b** shows a rapid onset of HDAC and Topo II inhibition activities which may be quickly lost due to diminished intracellular residency. The poor intracellular distribution of **12b** may suggest that the triazole-containing compounds **12a–d** are prone to efflux, in a similar manner to the anthracycline template. Alternatively, it may be that **12a–d** are not easily taken up into the cell. Either of these limitations would compromise the bioactivity of **12a–d** and may explain their less than optimal cytotoxic activity, despite evidence for potent inhibition of Topo II and HDACs. Nevertheless, the amide-containing compound **7** is a lead that merits additional study due primarily to its good intracellular distribution and potency that rivals DAU. It will be of interest to know how **7** fares with respect to common deleterious side effects that have plagued anthracycline therapy.

EXPERIMENTAL SECTION

Materials and General Methods. Suberic acid, 4-aminobenzyl alcohol, and 4-ethynylbenzyl alcohol were purchased from Sigma–Aldrich. Anhydrous solvents and other reagents were purchased and used without further purification. Analtech silica gel plates (60 F254) were used for analytical TLC, and Analtech preparative TLC plates (UV 254, 2000 μm) were used for purification. UV light was used to examine the spots. Silica gel (200–400 Mesh) was used in column chromatography. NMR spectra were recorded on a Varian-Gemini 400 magnetic resonance spectrometer. ¹H NMR spectra were recorded in parts per million (ppm) relative to the peak of CDCl₃ (7.24 ppm), CD₃OD (3.31 ppm), or DMSO-*d*₆ (2.49 ppm). ¹³C spectra were recorded relative to the central peak of the CDCl₃ triplet (77.0 ppm), CD₃OD (49.0 ppm), or the DMSO-*d*₆ septet (39.7 ppm) and were recorded with complete heterodecoupling. Multiplicities are described using the abbreviation: s, singlet; d, doublet; t, triplet; q, quartet; m, multiplet; and app, apparent. High-resolution mass spectra were recorded at the Georgia Institute of Technology mass spectrometry facility in Atlanta. The purity of all tested compounds was established by HPLC to be >95%. HPLC analyses were performed on a Beckman Coulter instrument using a Phenomenex RP C-18 column (250 mm \times 4.6 mm), eluting with solvent A (0.1% formic acid–water) and solvent B (0.1% formic acid–acetonitrile) at a gradient of 5–50% over 30 min, with detection at 498 nm and a flow rate of 1 mL/min. Sample concentrations were 250 μM , injecting 50 μL . *O*-Trityl-protected hydroxamates **9a–d**,⁴⁸ 4-ethynylbenzaldehyde **8**,⁶⁹ and suberic anhydride **2**⁷⁰ were prepared according to literature protocol.

8-(4-(Hydroxymethyl)phenylamino)-8-oxooctanoic Acid (3). To a stirring solution of suberic anhydride **2** (1.0 g, 6.40 mmol) in THF (15 mL) was added (4-aminophenyl)methanol **1** (0.78 g, 6.34 mmol), and resulting mixture was stirred at room temperature for 1 h. Ethyl acetate was added (60 mL), followed by washing with water (2 \times 50 mL), brine (1 \times 40 mL). Organic layer was dried on Na₂SO₄ and solvent evaporated under reduced pressure to give crude compound **2**, which was purified by column chromatography (silica, CH₂Cl₂–MeOH (step gradient, 0–10% methanol) to give 0.92 g of compound **3** (52%). ¹H NMR (DMSO-*d*₆, 400 MHz) δ 1.25–1.32 (4H, m), 1.49–1.61 (4H, m), 2.21 (2H, t, *J* = 7.2 Hz), 2.29 (2H, t, *J* = 8.0 Hz), 4.42 (2H, s), 5.10 (1H, s), 7.23 (2H, d, *J* = 8.4 Hz), 7.54 (2H, d, *J* = 8.8 Hz), 9.84 (1H, s), 12.0 (1H, s). ¹³C NMR (DMSO-*d*₆, 100 MHz) δ 24.4, 25.0, 28.3, 28.4, 33.6, 36.3, 62.5, 118.5, 126.6, 136.7, 137.7, 170.7, 174.1. HRMS (MALDI) calcd for C₁₅H₂₁NO₄Na [M + Na]⁺ 302.1363; found 302.1343.

8-(4-Formylphenylamino)-8-oxooctanoic Acid (4). To a stirring solution of alcohol **3** (1.71 g, 6.13 mmol) in CH₂Cl₂ was added Dess–Martin reagent (3.898 g, 9.19 mmol) at 0 °C. The reaction mixture

was stirred for the next 16 h at room temperature. The reaction was quenched by adding an aqueous solution of saturated sodium bicarbonate and saturated sodium thiosulfate (1:1, 40 mL) with stirring for 15 min. Methanol–CH₂Cl₂ 1:9 (70 mL) was added after the cessation of bubbling. The organic layer was isolated, washed subsequently with sodium bicarbonate–sodium thiosulfate mixture (1:1, 40 mL), brine (40 mL), and dried on Na₂SO₄. Solvent was evaporated under reduced pressure, and the crude product was purified by column chromatography using CH₂Cl₂–methanol (step gradient, 0–12% methanol) to give 1.10 g of compound **4** (65%). ¹H NMR (DMSO-*d*₆, 400 MHz) δ 1.24–1.30 (4H, m), 1.47 (2H, p, *J* = 7.2, 15.6 Hz), 1.56 (2H, p, *J* = 7.2, 14.0 Hz), 2.17 (2H, t, *J* = 7.6 Hz), 2.33 (2H, t, *J* = 7.2 Hz), 7.77–7.83 (4H, m), 9.84 (1H, s), 10.28 (1H, s), 11.99 (1H, s). ¹³C NMR (DMSO-*d*₆, 100 MHz) δ 24.3, 24.7, 28.3, 28.4, 33.6, 36.4, 118.6, 130.8, 131.0, 144.8, 172.0, 174.4, 191.5. HRMS (EI) calcd for C₁₅H₁₉NO₄ [M + H]⁺ 277.1314; found 277.1315.

***N*-(4-Formylphenyl)-*N*-(trityloxy)octanediamide (5).** Carboxylic acid **4** (0.30 g, 1.07 mmol) was dissolved in anhydrous THF. *N*-Methylmorpholine (0.12 mL, 1.07 mmol) was added to the solution. The reaction mixture was then cooled down to –15 °C and stirred for 5 min. Isobutylchloroformate (0.14 mL, 1.07 mmol) was added, and the mixture was stirred for 10 min at –15 °C. *O*-Tritylhydroxylamine (0.29 g, 1.07 mmol) was added, followed by 2 more equiv of *N*-methylmorpholine. Stirring continued for 15 min at –15 °C and 2 h at room temperature. Afterward, the mixture was poured into CH₂Cl₂ (50 mL) and water (50 mL). The organic layer was separated and extracted three times in each case with water, sodium bicarbonate solution (5%), and water. After washing with brine and drying over Na₂SO₄, solvent was evaporated in vacuo. Column chromatography with eluent system CH₂Cl₂–acetone (step gradient, 0–12% acetone) gave 0.37 g of compound **5** (66%) as a white solid. ¹H NMR (DMSO-*d*₆, 400 MHz) δ 1.10–1.21 (4H, m), 1.44–1.51 (2H, m), 1.73–1.77 (2H, m), 7.23–7.35 (15H, m), 7.78–7.84 (4H, m), 9.84 (1H, s), 10.16 (1H, s), 10.29 (1H, s). ¹³C NMR (DMSO-*d*₆, 100 MHz) δ 24.7, 28.3, 31.9, 36.4, 55.1, 91.5, 118.6, 127.4, 128.9, 130.9, 142.6, 144.6, 170.4, 172.1, 191.2. HRMS (ESI) calcd for C₃₄H₃₄N₂O₄Na [M + Na]⁺ 557.2207; found 557.2219.

***Daunorubicin-N-benzyl-4-amino-8-oxo-N*-(trityloxy)octanediamide (6).** A solution of daunorubicin (0.07 g, 0.12 mmol), aldehyde **5** (0.07 g, 0.12 mmol), and diisopropylethylamine (0.03 mL, 0.25 mmol) in DMF (2.5 mL) and MeOH (2.5 mL) was heated at 70 °C for 3 h and then allowed to cool to room temperature. Sodium cyanoborohydride (0.03 g, 0.50 mmol) was added, and stirring was continued at 70 °C for additional 24 h and allowed to cool at ambient temperature. The reaction was partitioned between CH₂Cl₂ (30 mL) and 5% NaHCO₃ (25 mL). The two layers were separated, and the aqueous layer was extracted with CH₂Cl₂ (2 \times 30 mL). The combined organic layer was washed with water (2 \times 30 mL) and brine (1 \times 20 mL) and dried over Na₂SO₄. Solvent was evaporated off and crude was purified on preparative TLC plates, eluting with mixture of CH₂Cl₂–MeOH (12:1) to give 0.05 g of compound **6** (38%). ¹H NMR (DMSO-*d*₆, 400 MHz) δ 0.93–0.98 (3H, m), 1.04–1.21 (8H, m), 1.38–1.53 (4H, m), 1.60–1.64 (2H, m), 1.71–1.75 (2H, m), 2.06–2.18 (4H, m), 2.24 (3H, s), 2.80–2.98 (3H, m), 3.15 (1H, d, *J* = 4.4 Hz), 3.57 (1H, s), 3.67–3.70 (1H, m), 4.05 (1H, q, *J* = 6.4, 12.8 Hz), 4.91 (1H, t, *J* = 4.4 Hz), 5.21 (1H, s), 5.42 (1H, s), 7.17 (2H, d, *J* = 8.4 Hz), 7.25–7.34 (15H, m), 7.42 (2H, d, *J* = 8.0 Hz), 7.58–7.62 (1H, m), 7.85–7.87 (2H, m), 9.70 (1H, s), 10.12 (1H, s). ¹³C NMR (CD₃OD, 100 MHz) δ 17.0, 24.7, 25.1, 25.5, 28.4, 29.6, 30.0, 30.9, 33.1, 34.8, 37.2, 49.7, 52.5, 56.5, 66.6, 66.7, 67.9, 69.7, 100.8, 111.1, 111.3, 118.3, 119.6, 119.8, 120.7, 127.7, 128.0, 128.6, 128.9, 134.2, 134.3, 135.3, 135.6, 137.2, 141.0, 155.7, 156.3, 160.9, 171.5, 186.5, 186.8, 211.8. HRMS (MALDI) calcd for C₆₁H₆₄N₃O₁₃ [M + H]⁺ 1046.4439; found 1046.4415.

Daunorubicin-N-benzyl-4-amino-8-oxooctahydroxamic Acid (7). To a solution of trityl-protected compound **6** (0.025 g, 0.024 mmol) in CH₂Cl₂–MeOH (1:1, 4 mL) was added BF₃·OEt₂ (0.05 mL) at room temperature. The reaction mixture stirred for 30 min at room temperature. Reaction was quenched by addition of water (25 mL) and 10% MeOH in CH₂Cl₂ (30 mL). The aqueous layer was isolated,

and its pH was adjusted to 8–9 by addition of satd NaHCO₃. This aqueous layer was then extracted with 10% MeOH in CH₂Cl₂ (3 × 30 mL). The combined organic layer was washed with satd brine and dried over Na₂SO₄, and the solvent was evaporated under reduced pressure. Trituration of crude product with CH₂Cl₂ (20 mL) gave pure 0.013 g of **7** (68%) as red solid. Retention time 6.46 min (solvent gradient: 5–60% solvent B over 20 min). ¹H NMR (CD₃OD, 400 MHz) δ 1.28–1.33 (9H, m), 1.50–1.60 (4H, m), 1.79–1.85 (1H, m), 1.93–1.94 (1H, m), 2.04–2.12 (2H, m), 2.23–2.30 (3H, m), 2.34 (3H, s), 2.85–3.08 (5H, m), 3.69–3.83 (3H, m), 3.97 (3H, s), 4.18–4.23 (1H, m), 5.04 (1H, s), 5.40 (1H, s), 7.22 (2H, d, *J* = 7.6 Hz), 7.39 (2H, d, *J* = 8.4), 7.47 (1H, d, *J* = 8 Hz), 7.74 (1H, t, *J* = 8 Hz), 7.82 (1H, d, *J* = 7.2 Hz). ¹³C NMR (CDCl₃ with drops of CD₃OD, 100 MHz) δ 17.2, 24.7, 26.2, 26.3, 29.5, 29.6, 30.4, 33.2, 33.5, 36.4, 37.6, 53.3, 54.4, 57.0, 67.5, 68.2, 71.1, 77.2, 101.7, 111.8, 112.1, 115.3, 119.8, 120.3, 121.0, 121.2, 128.3, 130.1, 135.3, 135.4, 136.0, 136.8, 139.2, 155.9, 157.1, 162.0, 172.5, 174.1, 187.3, 187.7, 213.5. HRMS (MALDI) calcd for C₄₂H₅₀N₃O₁₃ [M + H]⁺ 804.3343, found 804.336, and calcd for [M + Na]⁺ 826.3163, found 826.3153.

Representative Procedure for Cu(I)-Catalyzed Cycloaddition Reaction: O-Trityl-4-formylphenyltriazolylpentahydroxamate (10a). 5-Azido-O-tritylpentahydroxamate **9a** (0.15 g, 0.37 mmol) and 4-ethynylbenzaldehyde **8** (0.06 g, 0.49 mmol) were dissolved in anhydrous THF (10 mL) and stirred under argon at room temperature. Copper(I) iodide (9 mg, 0.05 mmol) and Hunig's base (0.1 mL) were then added to the reaction mixture, and stirring continued for 24 h. The reaction mixture was diluted with CH₂Cl₂ (30 mL) and washed with 1:4 NH₄OH–satd NH₄Cl (3 × 30 mL) and satd NH₄Cl (30 mL). The organic layer was dried over Na₂SO₄ and concentrated in vacuo. The crude product was purified by flash chromatography (CH₂Cl₂–acetone, gradient 12:1, 10:1, 8:1) to give 0.16 g of **10a** (82%) as a white solid. ¹H NMR (DMSO-*d*₆, 400 MHz) δ 1.13–1.20 (2H, m), 1.49–1.56 (2H, m), 1.82 (2H, t, *J* = 7.2), 4.27 (2H, t, *J* = 6.8 Hz), 7.24–7.28 (15H, m), 7.97 (2H, d, *J* = 8.8 Hz), 8.05–8.07 (2H, d, *J* = 8.4 Hz), 8.68 (1H, s), 9.99 (1H, s), 10.23 (1H, s). ¹³C NMR (CDCl₃, 100 MHz) δ 20.0, 29.2, 30.1, 50.0, 93.4, 120.8, 125.8, 127.7, 128.0, 128.8, 130.2, 135.5, 136.3, 140.8, 146.1, 176.2, 191.6. HRMS (MALDI) calcd for C₃₃H₃₀N₄O₃Na [M + Na]⁺ 553.2210; found 553.2191.

O-Trityl-4-formylphenyltriazolylhexahydroxamate (10b). Reaction of 6-azido-O-tritylhexahydroxamate **9b** (0.24 g, 0.58 mmol) and 4-ethynylbenzaldehyde **8** (0.09 g, 0.69 mmol) as described for the synthesis of **10a**, followed by purification using column chromatography (CH₂Cl₂–acetone, gradient 12:1, 10:1, 8:1) gave 0.19 g of **10b** (61%) as a white solid. ¹H NMR (DMSO-*d*₆, 400 MHz) δ 0.92–0.99 (2H, m), 1.19–1.26 (2H, m), 1.70–1.78 (4H, m), 4.30 (2H, t, *J* = 6.8), 7.26–7.29 (15H, m), 7.96 (2H, d, *J* = 8.0 Hz), 8.05 (2H, d, *J* = 8.4 Hz), 8.72 (1H, s), 9.99 (1H, s), 10.15 (1H, s). ¹³C NMR (CDCl₃, 100 MHz) δ 22.2, 25.5, 29.6, 30.7, 49.9, 93.1, 120.8, 125.7, 127.6, 127.9, 128.8, 130.1, 135.4, 136.3, 140.7, 141.6, 146.0, 176.5, 191.5.

O-Trityl-4-formylphenyltriazolylheptahydroxamate (10c). Reaction of 7-azido-O-tritylheptahydroxamate **9c** (0.30 g, 0.70 mmol) and 4-ethynylbenzaldehyde **8** (0.09 g, 0.70 mmol) as described for the synthesis of **10a**, followed by purification using column chromatography (CH₂Cl₂–acetone, gradient 12:1, 10:1, 8:1) gave 0.25 g of **10c** (65%) as a white solid. ¹H NMR (DMSO-*d*₆, 400 MHz) δ 0.96–1.17 (6H, m), 1.71–1.78 (4H, m), 4.34 (2H, t, *J* = 7.2 Hz), 7.24–7.34 (15H, m), 7.96 (2H, d, *J* = 7.6 Hz), 8.06 (2H, d, *J* = 8.0 Hz), 8.75 (1H, s), 9.99 (1H, s), 10.14 (1H, s). ¹³C NMR (CDCl₃, 100 MHz) δ 22.8, 25.8, 28.0, 29.7, 30.7, 50.1, 93.2, 120.7, 125.7, 127.9, 128.8, 130.1, 135.4, 136.3, 140.8, 141.7, 146.1, 176.8, 191.5.

O-Trityl-4-formylphenyltriazolyl-octahydroxamate (10d). Reaction of 8-azido-O-trityloctahydroxamate **9d** (0.25 g, 0.57 mmol) and 4-ethynylbenzaldehyde **8** (0.07 g, 0.57 mmol) as described for the synthesis of **10a**, followed by purification using column chromatography (CH₂Cl₂–acetone, gradient 12:1, 10:1, 8:1) gave 0.19 g of **10d** (59%) as a white solid. ¹H NMR (DMSO-*d*₆, 400 MHz) δ 0.85–0.93 (2H, m), 1.08–1.17 (6H, m), 1.72–1.80 (4H, m), 4.38 (2H, t, *J* = 7.2), 7.24–7.28 (15H, m), 7.96 (2H, d, *J* = 7.6 Hz), 8.06 (2H, d, *J* = 8.0 Hz), 8.77 (1H, s), 9.99 (1H, s), 10.13 (1H, s). ¹³C NMR (CDCl₃, 100 MHz) δ 23.0, 26.0, 28.3, 28.5, 30.0, 30.8, 50.3, 93.1, 120.7, 125.8,

127.9, 128.8, 130.2, 135.4, 136.3, 140.8, 141.7, 146.1, 176.9, 191.5. HRMS (MALDI) calcd for C₃₆H₃₆N₄O₃Na [M + Na]⁺ 595.2679; found 595.2609.

Daunorubicin-N-benzyl-4-triazolyl-O-tritylpentahydroxamate (11a). A solution of daunorubicin hydrochloride (0.08 g, 0.14 mmol) and **10a** (0.15 g, 0.28 mmol) in acetonitrile (9 mL) and water (3 mL) was stirred at room temperature for 30 min. A suspension of sodium cyanoborohydride in THF was added within 1 min, and stirring continued overnight at room temperature during which all of the starting material got consumed. The reaction mixture was partitioned between CH₂Cl₂ (30 mL) and water (30 mL), and the two layers were separated. The aqueous layer was extracted with CH₂Cl₂ (30 mL), and the combined organic layer was dried over Na₂SO₄. Solvent was removed under reduced pressure, and the crude was purified by preparative TLC, eluting with 12:1 CH₂Cl₂–MeOH to give 0.065 g of **11a** (44%) as red solid. ¹H NMR (DMSO-*d*₆, 400 MHz) δ 1.23–1.27 (5H, m), 1.36 (3H, d, *J* = 6.4 Hz), 1.60–1.68 (5H, m), 1.76–1.83 (2H, m), 2.10–2.15 (1H, m), 2.34–2.39 (1H, m), 2.88–2.93 (1H, m), 2.99–3.03 (1H, m), 3.21–3.26 (1H, m), 3.64 (1H, s), 3.67–3.70 (1H, m), 3.79–3.83 (1H, m), 3.97 (1H, q, *J* = 6.4 Hz), 4.06 (3H, s), 4.16–4.19 (2H, m), 4.73 (1H, s), 4.76 (1H, s), 5.30 (1H, s), 5.51 (1H, d, *J* = 3.2 Hz), 7.26–7.33 (15H, m), 7.36–7.42 (3H, m), 7.64 (1H, s), 7.71 (2H, d, *J* = 8.0 Hz), 7.76 (1H, t, *J* = 8.4 Hz), 8.01 (1H, d, *J* = 7.2 Hz). ¹³C NMR (CDCl₃, 100 MHz) δ 17.4, 20.4, 29.7, 29.9, 30.4, 34.2, 35.7, 50.2, 50.3, 52.5, 56.9, 65.7, 67.0, 67.1, 69.5, 101.0, 111.6, 111.7, 118.6, 119.6, 120.0, 121.1, 126.0, 127.4, 128.1, 128.4, 128.7, 129.2, 129.9, 133.8, 134.0, 135.7, 136.0, 139.6, 141.1, 155.9, 156.4, 161.3, 186.9, 187.3, 213.9. HRMS (ESI) calcd for C₆₀H₆₀N₃O₁₂ [M + H]⁺ 1042.4233; found 1042.4189.

Daunorubicin-N-benzyl-4-triazolyl-O-tritylhexahydroxamate (11b). Reaction of daunorubicin hydrochloride (0.055 g, 0.097 mmol) with **10b** (0.159 g, 0.29 mmol) and sodium cyanoborohydride (0.018 g, 0.29 mmol) in acetonitrile–water solvent system, as described in the synthesis of **11a**, gave 0.05 g of **11b** (49%) as red solid. ¹H NMR (DMSO-*d*₆, 400 MHz) δ 1.23–1.28 (5H, m), 1.38 (3H, d, *J* = 6.4 Hz), 1.56–1.60 (3H, m), 1.66–1.85 (6H, m), 2.12–2.17 (1H, m), 2.35–2.41 (1H, m), 2.91–2.94 (1H, m), 2.99–3.04 (1H, m), 3.23–3.28 (1H, m), 3.66–3.72 (2H, m), 3.81–3.84 (1H, m), 3.99 (1H, q, *J* = 6.8 Hz), 4.07 (3H, s), 4.28 (2H, t, *J* = 7.6 Hz), 4.74 (1H, s), 4.78 (1H, s), 5.29–5.32 (1H, m), 5.53 (1H, d, *J* = 2.8 Hz), 7.30–7.35 (15H, m), 7.37–7.45 (3H, m), 7.67 (1H, s), 7.73–7.80 (3H, m), 8.02 (1H, d, *J* = 7.2 Hz). ¹³C NMR (CDCl₃, 100 MHz) δ 17.1, 22.5, 25.7, 29.6, 29.8, 30.2, 30.7, 33.9, 35.4, 49.9, 50.0, 52.3, 56.6, 65.4, 66.7, 66.8, 69.3, 100.8, 111.3, 111.5, 118.4, 119.4, 119.8, 120.8, 125.8, 127.8, 128.1, 128.4, 128.9, 129.7, 133.5, 133.8, 135.4, 135.7, 139.5, 141.1, 147.3, 155.6, 156.2, 161.0, 186.7, 187.0, 213.7. HRMS (ESI) calcd for C₆₁H₆₂N₃O₁₂ [M + H]⁺ 1056.4389; found 1056.4440.

Daunorubicin-N-benzyl-4-triazolyl-O-tritylheptahydroxamate (11c). Reaction of daunorubicin hydrochloride (0.055 g, 0.097 mmol) with **10c** (0.162 g, 0.29 mmol) and sodium cyanoborohydride (0.018 g, 0.29 mmol) in acetonitrile–water solvent system, as described in the synthesis of **11a**, gave 0.05 g of **11c** (48%) as a red solid. ¹H NMR (DMSO-*d*₆, 400 MHz) δ 0.99–1.07 (2H, m), 1.13–1.25 (6H, m), 1.36 (3H, d, *J* = 6.4 Hz), 1.52–1.57 (2H, m), 1.70–1.83 (5H, m), 2.02–2.10 (2H, m), 2.14 (1H, s), 2.33 (1H, s), 2.85–2.88 (1H, m), 2.93 (1H, s), 2.97–3.00 (1H, s), 3.14–3.19 (1H, m), 3.67–3.70 (2H, m), 3.80–3.83 (1H, m), 4.04 (3H, s), 4.28 (3H, t, *J* = 6.8 Hz), 4.66–4.69 (1H, m), 5.24 (1H, s), 5.50 (1H, d, *J* = 3.2 Hz), 7.26–7.30 (15H, m), 7.34–7.43 (3H, m), 7.63 (1H, s), 7.66–7.79 (3H, m), 7.97 (1H, d, *J* = 7.6 Hz). ¹³C NMR (CDCl₃, 100 MHz) δ 17.1, 23.1, 24.8, 25.9, 28.2, 29.7, 30.0, 30.9, 30.9, 33.2, 34.9, 49.9, 50.2, 52.3, 56.6, 66.6, 66.7, 69.9, 100.6, 111.3, 111.5, 118.4, 119.4, 119.9, 120.9, 125.7, 127.8, 128.1, 128.4, 128.9, 129.9, 134.2, 134.2, 135.4, 135.7, 139.5, 141.1, 147.3, 155.6, 156.2, 161.0, 186.7, 187.1, 212.0. HRMS (ESI) calcd for C₆₂H₆₄N₃O₁₂ [M + H]⁺ 1070.4546; found 1070.4508.

Daunorubicin-N-benzyl-4-triazolyl-O-trityloctahydroxamate (11d). Reaction of daunorubicin hydrochloride (0.055 g, 0.097 mmol) with **10d** (0.166 g, 0.29 mmol) and sodium cyanoborohydride (0.018 g, 0.29 mmol) in acetonitrile–water solvent system, as described in the synthesis of **11a**, gave 0.048 g of **11d** (46%) as a red solid. ¹H NMR

(DMSO- d_6 , 400 MHz) δ 0.98–1.06 (2H, m), 1.19–1.24 (8H, m), 1.37 (3H, d, $J = 6.4$ Hz), 1.53–1.58 (2H, m), 1.69–1.85 (5H, m), 2.07–2.10 (2H, m), 2.35 (1H, s), 2.88–2.92 (1H, m), 2.96–2.99 (1H, m), 3.15–3.20 (1H, m), 3.67–3.70 (2H, m), 3.79–3.83 (1H, m), 4.05 (3H, s), 4.31 (3H, t, $J = 6.8$ Hz), 4.68 (1H, s), 5.25 (1H, s), 5.50 (1H, s), 7.27–7.31 (15H, m), 7.35–7.47 (3H, m), 7.66 (1H, s), 7.69–7.77 (3H, m), 7.98 (1H, d, $J = 7.6$ Hz). ^{13}C NMR (CDCl_3 , 100 MHz) δ 17.0, 23.1, 24.8, 26.1, 28.5, 29.6, 30.1, 30.2, 31.0, 33.2, 34.8, 50.0, 50.2, 52.5, 56.6, 66.5, 66.7, 69.8, 100.9, 111.1, 111.2, 118.3, 119.2, 119.7, 120.7, 125.7, 127.8, 128.0, 128.4, 128.9, 129.6, 134.2, 134.3, 135.4, 135.6, 139.5, 141.0, 147.3, 155.7, 156.3, 160.9, 186.5, 186.8, 211.8. HRMS (ESI) calcd for $\text{C}_{63}\text{H}_{66}\text{N}_5\text{O}_{12}$ $[\text{M} + \text{H}]^+$ 1084.4702; found 1084.4657.

Daurorubicin-N-benzyl-4-triazolypentahydroxamic Acid (12a). Reaction of **11a** (0.05 g, 0.048 mmol) and $\text{BF}_3 \cdot \text{OEt}_2$ (0.1 mL) in CH_2Cl_2 -MeOH (4 mL/4 mL) within 2 h, as described for the synthesis of **7**, followed by preparative TLC (eluent, CH_2Cl_2 -MeOH 7:1) to give 0.028 g of **12a** (73%) as red solid. Retention time 15.06 min (solvent gradient: 0–100% solvent B over 30 min). ^1H NMR (DMSO- d_6 , 400 MHz) δ 1.11–1.21 (7H, m), 1.42–1.50 (4H, m), 1.74–1.80 (2H, m), 1.96 (2H, t, $J = 7.6$ Hz), 2.06–2.22 (5H, m), 2.84–2.97 (3H, m), 3.63–3.80 (1H, m), 3.96 (3H, s), 4.07–4.09 (1H, m), 4.33 (2H, t, $J = 6.8$ Hz), 4.91 (1H, m), 5.22 (1H, s), 5.47 (1H, s), 7.37 (2H, d, $J = 8.0$ Hz), 7.61–7.63 (1H, m), 7.69–7.71 (2H, d, $J = 8.0$ Hz), 7.87–7.92 (2H, m), 8.46 (1H, s), 10.37 (1H, s). ^{13}C NMR (CDCl_3 with drops of CD_3OD , 125 MHz) δ 15.1, 22.5, 24.1, 24.2, 27.3, 27.4, 28.3, 31.0, 31.3, 34.2, 35.4, 51.1, 52.2, 54.8, 65.4, 66.1, 68.9, 75.1, 99.5, 109.7, 109.9, 113.1, 117.6, 118.2, 118.8, 119.0, 126.3, 127.9, 133.1, 133.2, 133.8, 134.7, 137.0, 153.7, 154.9, 159.8, 170.4, 172.0, 185.1, 185.5, 211.1. HRMS (ESI) calcd for $\text{C}_{41}\text{H}_{46}\text{N}_5\text{O}_{12}$ $[\text{M} + \text{H}]^+$ 800.3137; found 800.3088.

Daurorubicin-N-benzyl-4-triazolylhexahydroxamic Acid (12b). Reaction of **11b** (0.05 g, 0.047 mmol) and $\text{BF}_3 \cdot \text{OEt}_2$ (0.1 mL) in CH_2Cl_2 -MeOH (4 mL/4 mL) within 2 h, as described for the synthesis of **7**, followed by preparative TLC (eluent, CH_2Cl_2 -MeOH 7:1) gave 0.028 g of **12b** (76%) as red solid. Retention time 15.20 min (solvent gradient: 0–100% solvent B over 30 min). ^1H NMR ($\text{CDCl}_3 + \text{CD}_3\text{OD}$, 400 MHz) δ 0.74–0.84 (2H, m), 1.25–1.31 (7H, m), 1.54–1.62 (3H, m), 1.72–1.73 (2H, m), 1.83–1.93 (2H, m), 1.99 (1H, t, $J = 7.6$ Hz), 2.03–2.08 (1H, m), 2.19–2.33 (2H, m), 3.57–3.60 (5H, m), 3.68–3.73 (2H, m), 4.00 (3H, s), 4.30 (2H, q, $J = 7.2$ Hz), 4.65–4.66 (1H, m), 5.22–5.23 (1H, m), 5.44 (1H, s), 7.24–7.25 (1H, m), 7.34 (2H, d, $J = 8.4$ Hz), 1.61–1.65 (2H, m), 7.70–7.72 (1H, m), 7.74–7.75 (1H, m), 7.95 (1H, d, $J = 7.6$ Hz). ^{13}C NMR (CDCl_3 with drops of CD_3OD , 100 MHz) δ 16.8, 22.5, 24.3, 25.4, 29.5, 30.7, 32.2, 33.6, 35.3, 50.0, 50.1, 51.9, 56.5, 65.0, 67.0, 67.2, 69.0, 100.6, 111.3, 111.4, 118.4, 119.7, 119.9, 125.7, 127.8, 128.6, 129.1, 133.7, 133.8, 135.3, 135.7, 147.3, 160.9, 170.2, 186.7, 187.1, 213.5. HRMS (ESI) calcd for $\text{C}_{42}\text{H}_{48}\text{N}_5\text{O}_{12}$ $[\text{M} + \text{H}]^+$ 814.3294; found 814.3323.

Daurorubicin-N-benzyl-4-triazolylheptahydroxamic Acid (12c). Reaction of **11c** (0.05 g, 0.047 mmol) and $\text{BF}_3 \cdot \text{OEt}_2$ (0.1 mL) in CH_2Cl_2 -MeOH (4 mL/4 mL) within 2 h, as described for the synthesis of **7**, followed by preparative TLC (eluent, CH_2Cl_2 -MeOH 7:1) gave 0.030 g of **12c** (78%) as red solid. Retention time 16.98 min (solvent gradient: 5–60% solvent B over 20 min). ^1H NMR (DMSO- d_6 , 400 MHz) δ 1.17–1.26 (8H, m), 1.37–1.49 (3H, m), 1.70–1.83 (5H, m), 1.89–1.92 (1H, m), 1.99 (1H, t, $J = 7.2$ Hz), 2.09–2.23 (5H, m), 2.83–2.99 (4H, m), 3.63–3.84 (2H, m), 3.92–3.96 (3H, m), 4.08 (1H, t, $J = 6.8$ Hz), 4.31 (2H, t, $J = 6.8$ Hz), 4.93–4.96 (1H, m), 5.25 (1H, s), 5.34 (1H, s), 7.36 (2H, d, $J = 8.0$ Hz), 7.53–7.60 (1H, m), 7.70 (2H, d, $J = 8.0$ Hz), 7.79–7.80 (1H, m), 7.85–7.86 (1H, m), 8.41 (1H, s), 10.21 (1H, s). ^{13}C NMR (DMSO- d_6 , 100 MHz) δ 17.7, 24.6, 25.5, 25.8, 26.1, 26.2, 27.2, 28.4, 28.6, 28.6, 30.1, 32.4, 32.8, 37.0, 50.1, 57.3, 67.4, 70.7, 76.1, 101.2, 111.5, 119.8, 120.6, 120.9, 121.8, 125.6, 128.6, 129.0, 129.5, 135.6, 136.4, 136.9, 146.8, 155.2, 155.9, 161.7, 186.8, 212.0. HRMS (ESI) calcd for $\text{C}_{43}\text{H}_{50}\text{N}_5\text{O}_{12}$ $[\text{M} + \text{H}]^+$ 828.3450; found 828.3407.

Daurorubicin-N-benzyl-4-triazolyl-octahydroxamic Acid (12d). Reaction of **11d** (0.05 g, 0.046 mmol) and $\text{BF}_3 \cdot \text{OEt}_2$ (0.1 mL) in

CH_2Cl_2 -MeOH (4 mL/4 mL) within 2 h, as described for the synthesis of **7**, followed by preparative TLC (eluent, CH_2Cl_2 -MeOH 7:1), gave 0.028 g of **12d** (73%) as red solid. Retention time 16.93 min (solvent gradient: 5–60% solvent B over 20 min). ^1H NMR (DMSO- d_6 , 400 MHz) δ 1.15–1.20 (8H, m), 1.41–1.44 (2H, m), 1.64–1.67 (2H, m), 1.77–1.80 (2H, m), 1.88 (2H, t, $J = 7.6$), 1.95–1.20 (2H, m), 2.23–2.24 (3H, m), 2.80–2.94 (3H, m), 3.60–3.67 (2H, m), 3.76–3.79 (1H, m), 3.89–3.94 (3H, m), 4.05–4.10 (1H, m), 4.30 (2H, t, $J = 7.2$), 4.88–4.91 (1H, m), 5.21 (1H, m), 5.42 (1H, s), 7.33–7.35 (2H, m), 7.57–7.59 (1H, m), 7.65–7.73 (2H, m), 7.83–7.86 (2H, m), 8.44 (1H, s), 10.29 (1H, m). ^{13}C NMR (DMSO- d_6 , 125 MHz) δ 17.2, 24.0, 24.8, 25.5, 27.9, 29.4, 30.8, 31.5, 32.1, 36.2, 48.4, 49.3, 51.8, 54.8, 56.5, 66.8, 70.0, 75.1, 75.2, 100.6, 110.5, 110.6, 118.8, 119.5, 119.9, 120.8, 124.9, 128.3, 129.1, 134.4, 134.6, 135.5, 136.1, 146.2, 154.1, 155.8, 160.6, 169.0, 186.3, 211.5. HRMS (ESI) calcd for $\text{C}_{44}\text{H}_{50}\text{N}_5\text{O}_{12}$ $[\text{M} + \text{H}]^+$ 842.3607; found 842.3626.

In Vitro HDAC Inhibition. In vitro HDAC inhibition was assayed using the HDAC Fluorimetric Assay/Drug Discovery Kit as previously described.⁴⁸ Briefly, 15 μL of HeLa nuclear extract was mixed with 5 μL of 10 \times compound and 5 μL of assay buffer. Fluorogenic substrate (25 μL) was added, and reaction was allowed to proceed for 15 min at room temperature and then stopped by addition of a developer containing TSA. Fluorescence was monitored after 15 min at excitation and emission wavelengths of 360 and 460 nm, respectively. IC_{50} values were determined using logit plots.

KDNA Decatenation Assay. The decatenation of KDNA was assayed according to TopoGen protocol in order to determine topoisomerase II activity. The substrate KDNA (200 ng) and 50 μM drug were combined in assay buffer (50 mM Tris-HCl, pH 8, 120 mM KCl, 10 mM MgCl_2 , 0.5 mM ATP, 0.5 mM dithiothreitol, 300 $\mu\text{g}/\text{mL}$ bovine serum albumin (BSA)) and incubated for 10 min on ice. Next, 1 U of topoisomerase II was added and the reaction was allowed to proceed for 10 min at 37 $^\circ\text{C}$. The reaction was quenched via the addition of loading buffer (1% sarkosyl, 0.025% bromophenol blue, and 5% glycerol) and was then analyzed by electrophoresis on a 1% agarose gel in TBE buffer (89 mM Tris, 89 mM borate, and 2 mM Na-EDTA, pH 8.3) for 3.5 h at 40 V. The gel was stained with SYBR Green I (Molecular Probes) for 30 min and was visualized under UV illumination and photographed on an AlphaImager.

Cellular Topo II Inhibition. DU-145 cells were probed for Topo II inhibition with an in vitro blotting kit designed to show relative amounts of stabilized Topo II-DNA cleavage complexes (Topoisomerase II In Vivo Link Kit, Topogen). Briefly, cells were dosed with Topo II-HDACi's at concentrations pertaining to their respective IC_{50} values for cell viability inhibition. Control cells were dosed with 0.1% DMSO to take into account DMSO from stock solutions of drug. As recommended in the protocol instructions, cells were dosed for 30 min, counted, and lysed with 1% sarkosyl. Alternately, DU-145 cells were dosed for 72 h, counted, and equalized with the cell count from the 30 min incubation before subsequent lysis. Lysate was collected, loaded on a CsCl gradient, and subjected to centrifugation at 31000 rpm at room temperature for 12 h. Aliquots of the gradient separations were then taken and the Topo II-DNA cleavage complexes were identified via absorbance at 260 nm. Aliquots were then loaded into a slot blotting device and subjected to vacuum to load proteins onto a nitrocellulose membrane. Immunoblotting using the Odyssey Imaging System (LiCor Biosciences) revealed Topo II levels associated with the stabilized DNA complexes.

Cell Culture and Viability. DU-145 prostate carcinoma and SK-MES-1 nonsmall cell lung carcinoma was obtained from ATCC (Manassass, VA) and maintained in the recommended growth mediums. MCF-7 breast cancer cells were a generous gift from Dr. Donald Doyle. All cell lines were maintained in a 37 $^\circ\text{C}$ incubator with a 5% CO_2 environment. All compounds to be tested were dissolved to a concentration of 10 mM in DMSO and stored at -80 $^\circ\text{C}$. Cells were passaged 24 h prior to cell viability experiments. For cancer cell viability experiments, cells were dosed for 72 h and viability was determined through the use of the MTS assay (Promega) according to manufacturer's instructions. Control wells were dosed with fresh media containing 0.1% DMSO.

Western Blot of p21^{waf1} Expression and Histone Hyperacetylation. DU-145 prostate cancer cells were passaged 24 h prior to the experiment. Compounds to be tested were diluted in the growth medium so that the final concentration of DMSO was 0.1% and control cells were dosed with fresh media containing 0.1% DMSO. Cells were dosed for 24 h then washed twice with ice-cold PBS and lysed on the culture plate at 4 °C for 5 min with RIPA buffer containing protease inhibitors. Lysates were mixed repeatedly by pipetting and centrifuged at 14000g for 15 min at 4 °C. Supernatant was saved and protein concentration was quantified using the Bio-Rad Protein Assay (Bio-Rad) with BSA as the standard. Loading buffer was added, and protein samples were incubated at 100 °C for 10 min before electrophoresis. Proteins were then transferred to a nitrocellulose membrane for 1 h, followed by blocking overnight in a 1:1 mixture of Odyssey Blocking Buffer (LiCor Biosciences) and PBS. Membranes were incubated with primary and secondary antibodies, both diluted in 1:1 Odyssey Blocking Buffer/PBS. Membranes were scanned on the Odyssey infrared imaging system (LiCor Biosciences) using both 700 and 800 nm channels simultaneously at 169 μm resolution and analyzed on the imaging software.

Western Blot of Tubulin Acetylation. DU-145 cells were passaged 24 h prior to dosing. Compounds were diluted such that cells, including controls, were exposed to no more than 0.1% DMSO. Cells were dosed for 4 h before lysis in RIPA buffer with protease inhibitors. Lysates were vortexed and centrifuged at 14000 rpm at 4 °C for 15 min. Supernatants were removed, and protein concentration was assayed using the Bio Rad Protein Assay with BSA as a standard. Electrophoresis and immunoblotting were performed as described above. Rabbit antitubulin (Sigma) and mouse antiacetyl tubulin (Invitrogen) were used to probe the membrane after blocking with Odyssey blocking buffer (Li Cor). Li Cor near-infrared secondary antibodies were used to image the blot with the Odyssey infrared imaging system at 700 and 800 nm.

Confocal Microscopy. Cells were plated on glass coverslips in 35 mm dishes 24 h before the experiment. They were then incubated with fresh media containing the indicated compounds at concentration of 1 μM . After 4 h, cells were washed with PBS. Coverslips were then mounted and viewed under a confocal microscope (DAU λ_{ex} = 488 nm; Zeiss LSM 510 UV confocal microscope).

■ ASSOCIATED CONTENT

■ Supporting Information

¹H NMR and ¹³C NMR spectral information, HPLC traces, and molecular modeling outputs. This material is available free of charge via the Internet at <http://pubs.acs.org>.

■ AUTHOR INFORMATION

■ Corresponding Author

*Phone: 404-894-4047. Fax: 404-894-2291. E-mail: aoyelere@gatech.edu.

■ Author Contributions

[§]These authors contributed equally to the manuscript.

■ ACKNOWLEDGMENTS

We are grateful to Professor Olaf Wiest for providing us with the HDAC 1 homology model. This work was financially supported by NIH grant R01CA131217.

■ ABBREVIATIONS USED

HDAC, histone deacetylase; HAT, histone acetyltransferase; HDACi, histone deacetylase inhibitors; HDLP, histone deacetylase-like protein; SAHA, suberoylanilide hydroxamic acid; TSA, trichostatin A; DOX, doxorubicin; DAU, daunomycin; Topo II, topoisomerase II class of enzymes; KDNA, kinetoplast DNA

■ REFERENCES

- (1) Morphy, R.; Kay, C.; Rankovic, Z. From magic bullets to designed multiple ligands. *Drug Discovery Today* **2004**, *9*, 641–651.
- (2) Morphy, R.; Rankovic, Z. Designed Multiple Ligands. An Emerging Drug Discovery Paradigm. *J. Med. Chem.* **2005**, *48*, 6523–6543.
- (3) Frantz, S. Drug discovery: playing dirty. *Nature* **2005**, *437*, 942–943.
- (4) Roth, B. L.; Sheffler, D. J.; Kroeze, W. K. Magic shotguns versus magic bullets: selectively non-selective drugs for mood disorders and schizophrenia. *Nature Rev. Drug Discovery* **2004**, *3*, 353–359.
- (5) Hopkins, A. L.; Mason, J. S.; Overington, J. P. Can we rationally design promiscuous drugs? *Curr. Opin. Struct. Biol.* **2006**, *16*, 127–136.
- (6) Cmeserly, P.; Agoston, V.; Pongor, S. The efficiency of multi-target drugs: The network approach might help drug design. *Trends Pharmacol. Sci.* **2005**, *26*, 178–182.
- (7) Fray, M. J.; Bish, G.; Brown, A. D.; Fish, P. V.; Stobie, A.; Wakenhut, F.; Whitlock, G. A. *N*-(1,2-Diphenylethyl)piperazines: a new class of dual serotonin/noradrenaline reuptake inhibitor. *Bioorg. Med. Chem. Lett.* **2006**, *16*, 4345–4348.
- (8) Neumeyer, J. L.; Peng, X.; Knapp, B. I.; Bidlack, J. M.; Lazarus, L. H.; Salvadori, S.; Trapella, C.; Balboni, G. New opioid designed multiple ligand from Dmt-Tic and morphinan pharmacophores. *J. Med. Chem.* **2006**, *49*, 5640–5643.
- (9) Jones, P. A.; Baylin, S. B. The epigenomics of cancer. *Cell* **2007**, *128*, 683–692.
- (10) Kouzarides, T. Chromatin modifications and their function. *Cell* **2007**, *128*, 693–705.
- (11) Shilatifard, A. Chromatin modifications by methylation and ubiquitination: implications in the regulation of gene expression. *Annu. Rev. Biochem.* **2006**, *75*, 243–269.
- (12) Ropero, S.; Esteller, M. The role of histone deacetylases (HDACs) in human cancer. *Mol. Oncol.* **2007**, *1*, 19–25.
- (13) Marks, P. A.; Richon, V. M.; Rifkind, R. A. Histone deacetylase inhibitors: inducers of differentiation or apoptosis of transformed cells. *J. Natl. Cancer Inst.* **2000**, *92*, 1210–1216.
- (14) Saito, A.; Yamashita, T.; Mariko, Y.; Nosaka, Y.; Tsuchiya, K.; Ando, T.; Suzuki, T.; Tsuruo, T.; Nakanishi, O. A synthetic inhibitor of histone deacetylase, MS-275, with marked in vivo antitumor activity against human tumors. *Proc. Natl. Acad. Sci. U.S.A.* **1999**, *96*, 4592–4597.
- (15) Glick, R. D.; Swindemen, S. L.; Coffey, D. C.; Rifkind, R. A.; Marks, P. A.; Richon, V. M.; La Quaglia, M. P. Hybrid polar histone deacetylase induces apoptosis and CD95/CD95 ligand expression in human neuroblastoma. *Cancer Res.* **1999**, *59*, 4392–4399.
- (16) Butler, L. M.; Agus, D. B.; Scher, H. I.; Higgins, B.; Rose, A.; Cordon-Cardo, C.; Thaler, H. T.; Rifkind, R. A.; Marks, P. A.; Richon, V. M. Suberoylanilide hydroxamic acid, an inhibitor of histone deacetylase, suppresses the growth of prostate cancer cells in vitro and in vivo. *Cancer Res.* **2000**, *60*, 5165–5170.
- (17) Oyelere, A. K.; Chen, P. C.; Guerrant, W.; Mwakwari, S. C.; Hood, R.; Zhang, Y.; Fan, Y. Non-peptide macrocyclic histone deacetylase inhibitors. *J. Med. Chem.* **2009**, *52*, 456–468.
- (18) Gu, W.; Roeder, R. G. Activation of p53 sequence-specific DNA binding by acetylation of the p53 C-terminal domain. *Cell* **1997**, *90*, 595–606.
- (19) Martinez-Balbás, M. A.; Bauer, U. M.; Nielsen, S. J.; Brehm, A.; Kouzarides, T. Regulation of E2F1 activity by acetylation. *EMBO J.* **2000**, *19*, 662–671.
- (20) Marzio, G.; Wagener, C.; Gutierrez, M. I.; Cartwright, P.; Helin, K.; Giacca, M. E2F family members are differentially regulated by reversible acetylation. *J. Biol. Chem.* **2000**, *275*, 10887–10892.
- (21) Hubbert, C.; Guardiola, A.; Shao, R.; Kawaguchi, Y.; Ito, A.; Nixon, A.; Yoshida, M.; Wang, X. F.; Yao, T. P. HDAC6 is a microtubule-associated deacetylase. *Nature* **2002**, *417*, 455–458.
- (22) Kovacs, J. J.; Murphy, P. J.; Gaillard, S.; Zhao, X.; Wu, J. T.; Nicchitta, C. V.; Yoshida, M.; Toft, D. O.; Pratt, W. B.; Yao, T. P. HDAC6 regulates Hsp90 acetylation and chaperone-dependent activation of glucocorticoid receptor. *Mol. Cell* **2005**, *18*, 601–607.

- (23) Mann, B. S.; Johnson, J. R.; Cohen, M. H.; Justice, R.; Padzur, R. FDA approval summary: vorinostat for treatment of advanced primary cutaneous T-cell lymphoma. *Oncologist* **2007**, *12*, 1247–1252.
- (24) Grant, C.; Rahman, F.; Piekarz, R.; Peer, C.; Frye, R.; Robey, R. W.; Gardner, E. R.; Figg, W. D.; Bates, S. E. Romidepsin; a new therapy for cutaneous T-cell lymphoma and a potential therapy for solid tumors. *Expert Rev. Anticancer Ther.* **2010**, *10*, 997–1008.
- (25) Mwakwari, S. C.; Patil, V.; Guerrant, W.; Oyelere, A. K. Macrocyclic histone deacetylases inhibitors. *Curr. Top. Med. Chem.* **2010**, *10*, 1423–1440.
- (26) Kelly, W. K.; O'Connor, O. A.; Marks, P. A. Histone deacetylase inhibitors: from target to clinical trials. *Expert Opin. Invest. Drugs.* **2002**, *11*, 1695–1713.
- (27) Rosato, R. R.; Grant, S. Histone deacetylase inhibitors in clinical development. *Expert Opin. Invest. Drugs* **2004**, *13*, 21–38.
- (28) Yoo, C. B.; Jones, P. A. Epigenetic therapy of cancer: past, present and future. *Nature Rev. Drug Discovery* **2006**, *5*, 37–50.
- (29) Finnin, M. S.; Donigian, J. R.; Cohen, A.; Richon, V. M.; Rifkind, R. A.; Marks, P. A.; Breslow, R.; Pavletich, N. P. Structures of a histone deacetylase homologue bound to the TSA and SAHA inhibitors. *Nature* **1999**, *401*, 188–193.
- (30) Wang, D.-F.; Wiest, O.; Helquist, P.; Lan-Hargest, H.-Y.; Wiech, N. L. On the function of the 14 Å long internal cavity of histone deacetylase-like protein: implication for the design of histone deacetylase inhibitors. *J. Med. Chem.* **2004**, *47*, 3409–3417.
- (31) Chen, L.; Wilson, D.; Jayaram, H. N.; Pankiewicz, K. W. Dual inhibitors of inosine monophosphate dehydrogenase and histone deacetylases for cancer treatment. *J. Med. Chem.* **2007**, *50* (26), 6685–6691.
- (32) Mahboobi, S.; Dove, S.; Sellmer, A.; Winkler, M.; Eichhorn, E.; Pongratz, H.; Ciossek, T.; Baer, T.; Maier, T.; Beckers, T. Design of chimeric histone deacetylase- and tyrosine kinase-inhibitors: a series of iminatif hybrids as potent inhibitors of wild-type and mutant BCR-ABL, PDGF-R β , and histone deacetylases. *J. Med. Chem.* **2009**, *52* (8), 2265–2279.
- (33) Cai, X.; Zhai, H.-X.; Wang, J.; Forrester, J.; Qu, H.; Yin, L.; Cheng-Jung, L.; Bao, R.; Qian, C. Discovery of 7-(4-(3-ethynylphenylamino)-7-methoxyquinazolin-6-yloxy)-N-hydroxyheptanamide (CUDC-101) as a potent multi-acting HDAC, EGFR, and HER2 inhibitor for the treatment of cancer. *J. Med. Chem.* **2010**, *53* (5), 2000–2009.
- (34) Piccart-Gebhart, M. J. Anthracyclines and the tailoring of treatment for early breast cancer. *N. Engl. J. Med.* **2006**, *354*, 2177–2179.
- (35) Kim, M. S.; Blake, M.; Baek, J. H.; Kohlhagen, G.; Pommier, Y.; Carrier, F. Inhibition of histone deacetylase increases cytotoxicity to anticancer drugs targeting DNA. *Cancer Res.* **2003**, *63*, 7291–7300.
- (36) Catalano, M. G.; Fortunati, N.; Pugliese, M.; Poli, R.; Bosco, O.; Mastrocola, R.; Aragno, M.; Bocuzzi, G. Valproic acid, a histone deacetylase inhibitor, enhances sensitivity to doxorubicin in anaplastic thyroid cancer cells. *J. Endocrinol.* **2006**, *191* (2), 465–472.
- (37) Johnson, C. A.; Padget, K.; Austin, C. A.; Turner, B. M. Deacetylase activity associates with topoisomerase II and is necessary for etoposide-induced apoptosis. *J. Biol. Chem.* **2001**, *276* (7), 4539–4542.
- (38) Marchion, D. C.; Bicaku, E.; Daud, A. I.; Richon, V.; Sullivan, D. M.; Munster, P. N. Sequence-specific potentiation of topoisomerase II inhibitors by the histone deacetylase inhibitor suberoylanilide hydroxamic acid. *J. Cell Biochem.* **2004**, *92* (2), 223–237.
- (39) Tewey, K. M.; Rowe, T. C.; Yang, L.; Halligan, B. D.; Liu, L. F. Adriamycin-induced DNA damage mediated by mammalian DNA topoisomerase II. *Science* **1984**, *226*, 466–468.
- (40) Binaschi, M.; Bigioni, M.; Cipollone, A.; Rossi, C.; Goso, C.; Maggi, C. A.; Capranico, G.; Animati, F. Anthracyclines: selected new developments. *Curr. Med. Chem. Anti-Cancer Agents* **2001**, *1* (2), 113–130.
- (41) Pommier, Y.; Schwartz, R. E.; Kohn, K. W.; Zwelling, L. A. Formation and rejoining of deoxyribonucleic acid double-strand breaks induced in isolated nuclei by antineoplastic intercalating agents. *Biochemistry* **1984**, *23*, 3194–3201.
- (42) Kiyomiya, K.; Matsuo, S.; Kurebe, M. Proteasome is a carrier to translocate doxorubicin from cytoplasm into nucleus. *Life Sci.* **1998**, *62* (20), 1853–1860.
- (43) Kiyomiya, K.; Matsuo, S.; Kurebe, M. Mechanism of specific nuclear transport of adriamycin: the mode of nuclear translocation of adriamycin–proteasome complex. *Cancer Res.* **2001**, *61*, 2467–2471.
- (44) Tong, G. L.; Wu, H. Y.; Smith, T. H.; Henry, D. W. Adriamycin analogs. 3. Synthesis of N-alkylated anthracyclines with enhanced efficacy and reduced toxicity. *J. Med. Chem.* **1979**, *22*, 912–918.
- (45) Martín, B.; Vaquero, A.; Priebe, W.; Portugal, J. Bisanthracycline WP631 inhibits basal and Sp1-activated transcription initiated in vitro. *Nucleic Acids Res.* **1999**, *27*, 3402–3409.
- (46) Lothstein, L.; Israel, M.; Sweatman, T. W. Anthracycline drug targeting: cytoplasmic versus nuclear—a fork in the road. *Drug Resist. Updates* **2001**, *4*, 169–177.
- (47) Gate, L.; Couvreur, P.; Nguyen-Ba, G.; Tapiero, H. N-Methylation of anthracyclines modulates their cytotoxicity and pharmacokinetics in wild type and multidrug resistant cells. *Biomed. Pharmacother.* **2003**, *57*, 301–308.
- (48) (a) Mwakwari, S. C.; Guerrant, W.; Patil, V.; Khan, S. I.; Tekwani, B. L.; Gurard-Levin, Z. A.; Mrksich, M.; Oyelere, A. K. Non-peptide histone deacetylases inhibitors derived from tricyclic ketolide skeleton. *J. Med. Chem.* **2010**, *53*, 6100–6111. (b) Chen, P. C.; Patil, V.; Guerrant, W.; Green, P.; Oyelere, A. K. Synthesis and structure–activity relationship of histone deacetylase (HDAC) inhibitors with triazole-linked cap group. *Bioorg. Med. Chem.* **2008**, *16*, 4839–4853.
- (49) Lu, J.; Yoshida, O.; Hayashi, S.; Arimoto, H. Synthesis of rigidly-linked vancomycin dimers and their in vivo efficacy against resistant bacteria. *Chem. Commun.* **2007**, 251–253.
- (50) Preobrazhenskaya, M. N.; Olsufyeva, E. N.; Solovieva, S. E.; Tevyashova, A. N.; Reznikova, M. I.; Luzikov, Y. N.; Terekhova, L. P.; Trenin, A. S.; Galatenko, O. A.; Treshalin, I. D.; Mirchink, E. P.; Bukhman, V. M.; Sletta, H.; Zotchev, S. B. Chemical modification and biological evaluation of new semi-synthetic derivatives of 28, 29-didehydronystatin A₁ (S44HP), a genetically engineered anti-fungal polyene macrolide antibiotic. *J. Med. Chem.* **2009**, *52*, 189–196.
- (51) Yang, S.; Lagu, B.; Wilson, L. Mild and efficient lewis acid-promoted detritylation in the synthesis of N-hydroxy amides: a concise synthesis of (–)-cobactin T. *J. Org. Chem.* **2007**, *72* (21), 8123–8126.
- (52) Morris, G. M.; Goodsell, D. S.; Halliday, R. S.; Huey, R.; Hart, W. E.; Belew, R. K.; Olson, A. J. Automated docking using a Lamarckian genetic algorithm and empirical binding free energy function. *J. Comput. Chem.* **1998**, *19*, 1639–1662.
- (53) Estiu, G.; Wiest, O. HDAC1 homology model. Personal Communication.
- (54) Marini, J. C.; Miller, K. G.; Englund, P. T. Decatenation of kinetoplast DNA by topoisomerases. *J. Biol. Chem.* **1980**, *255* (11), 4976–4979.
- (55) Sahai, B.; Kaplan, J. A quantitative decatenation assay for type II topoisomerases. *Anal. Biochem.* **1986**, *156* (2), 364–379.
- (56) Qu, X.; Wan, C.; Becker, H. C.; Zhong, D.; Zewail, A. H. The anticancer drug–DNA complex: femtosecond primary dynamics for anthracycline antibiotics function. *Proc. Natl. Acad. Sci. U.S.A.* **2001**, *98* (25), 14212–14217.
- (57) Kulp, S. K.; Chen, C. S.; Wang, D. S.; Chen, C. Y.; Chen, C. S. Antitumor effects of a novel phenylbutyrate-based histone deacetylases inhibitor, (S)-HDAC-42, in prostate cancer. *Clin. Cancer Res.* **2006**, *12*, 5199–5206.
- (58) Doyle, L. A.; Abruzzo, Y. W.; Krogmann, T.; Yongming, G.; Rishi, A. K.; Ross, D. D. A multidrug resistance transporter from human MCF-7 breast cancer cells. *Proc. Natl. Acad. Sci. U.S.A.* **1998**, *95*, 15665–15670.
- (59) Richon, V. M.; Sandhoff, T. W.; Rifkind, R. A.; Marks, P. A. Histone deacetylase inhibitor selectively induces p21^{WAF1} expression and gene-associated histone acetylation. *Proc. Natl. Acad. Sci. U.S.A.* **2000**, *97* (18), 10014–10019.

(60) Gartenhaus, R. B.; Wang, P.; Hoffmann, P. Induction of the WAF1/CIP1 protein and apoptosis in human T-cell leukemia virus type I-transformed lymphocytes after treatment with adriamycin by using the p53-independent pathway. *Proc. Natl. Acad. Sci. U.S.A.* **1996**, *93*, 265–268.

(61) North, B. J.; Marshall, B. L.; Borra, M. T.; Denu, J. M.; Verdin, E. The human Sir2 ortholog, SIRT2, is an NAD⁺-dependent tubulin deacetylase. *Mol. Cell* **2003**, *11*, 437–444.

(62) Schäfer, S.; Saunders, L.; Eliseeva, E.; Velena, A.; Jung, M.; Schwienhorst, A.; Strasser, A.; Dickmanns, A.; Ficner, R.; Schlimme, S.; Sippl, W.; Verdin, E.; Jung, M. Phenylalanine-containing hydroxamic acids as selective inhibitors of class IIb histone deacetylases (HDACs). *Bioorg. Med. Chem.* **2008**, *16*, 2011–2033.

(63) Namdar, M.; Perez, G.; Ngo, L.; Marks, P. A. Selective inhibition of histone deacetylases 6 (HDAC6) induces DNA damage and sensitizes transformed cells to anticancer agents. *Proc. Natl. Acad. Sci. U.S.A.* **2010**, *107*, 20003–20008.

(64) Blagosklonny, M. V.; Robey, R.; Sackett, D. L.; Du, L.; Traganos, F.; Darzynkiewicz, Z.; Fojo, T.; Bates, S. E. Histone deacetylase inhibitors all induce p21 but differentially cause tubulin acetylation, mitotic arrest, and cytotoxicity. *Mol. Cell Ther.* **2002**, *1*, 937–941.

(65) Zhang, Y.; Li, N.; Caron, C.; Matthias, G.; Hess, D.; Khochbin, S.; Matthias, P. HDAC-6 interacts with and deacetylates tubulin and microtubules in vivo. *EMBO J.* **2003**, *22*, 1168–1179.

(66) Gao, H.; Huang, K. C.; Yamasaki, E. F.; Chan, K. K.; Chohan, L.; Snapka, R. M. XK469, a selective topoisomerase II β poison. *Proc. Natl. Acad. Sci. U.S.A.* **1999**, *96*, 12168–12173.

(67) Kiyomiya, K.; Satoh, J.; Horie, H.; Kurebe, M.; Nakagawa, H.; Matsuo, S. Correlation between nuclear action of anthracycline anticancer agents and their binding affinity to the proteasome. *Int. J. Oncol.* **2002**, *21* (5), 1081–1085.

(68) Marbeuf-Gueye, C.; Etti, D.; Priebe, W.; Kozłowski, H.; Garnier-Suillerot, A. Correlation between the kinetics of anthracycline uptake and the resistance factor in cancer cells expressing the multidrug resistance protein or the P-glycoprotein. *Biochim. Biophys. Acta* **1999**, *1450* (3), 374–384.

(69) Klyatskaya, S. V.; Tretyakov, E. V.; Vasilevsky, S. F. Cross-coupling of aryl iodides with paramagnetic terminal acetylenes derived from 4,4,5,5-tetramethyl-2-imidazoline-1-oxyl 3-oxide. *Russ. Chem. Bull.* **2002**, *51*, 128–134.

(70) Mai, A.; Esposito, M.; Sbardella, G.; Massa, S. A new facile and expeditious synthesis of *N*-hydroxy-*N'*-phenyloctanediamide, a potent inducer of terminal cytodifferentiation. *Org. Prep. Proced. Int.* **2001**, *33* (4), 391–394.